

Contents lists available at ScienceDirect

# Marine Structures

journal homepage: www.elsevier.com/locate/marstruc



# Effects of structural flexibility on the dynamic responses of low-height lifting mechanism for offshore wind turbine installation

Behfar Ataei <sup>a</sup>, Shuai Yuan <sup>a</sup>, Zhengru Ren <sup>b,\*</sup>, Karl Henning Halse <sup>a</sup>

- <sup>a</sup> Centre for Research-based innovation of Marine Operations (SFI MOVE), Department of Ocean Operations and Civil Engineering, Norwegian University of Science and Technology (NTNU), NO-6025 Aalesund, Norway
- <sup>b</sup> Institute for Ocean Engineering, Shenzhen International Graduate School, Tsinghua University, Tsinghua Campus, University
  Town, Shenzhen, 518055, China

#### ARTICLE INFO

# Keywords: Offshore wind turbine Low-height lifting Dynamic analysis Finite element method Crane structure flexibility

# ABSTRACT

Installation complexities are one of the major challenges in the floating offshore wind turbine (OWT) industry. The modern concept introduced by the SFI-MOVE project is an effort to overcome the complexities by utilizing a low-height lifting mechanism. It is common to idealize a crane in the lifting mechanism as a rigid body since the structural deflections are smaller than the responses introduced by the other system components. However, structural flexibility can play an essential role in demanding offshore operations with smaller acceptable tolerances. In this study, lifting cranes are modeled using the finite element method and simplified by implementing equivalent 3D beam elements. Dynamic analysis is performed for various environmental conditions, and the responses of the crane structure and the OWT are calculated for each load case. This research reveals that crane structure flexibility influences the relative motion between a floating spar buoy and an OWT during mating operations. Crane structural flexibility contributes significantly to the OWT rotations. In addition, the response deviation between using rigid and flexible cranes increases as the excitation force increases. Therefore, it is recommended to consider the crane structural flexibility in the calculation when strict installation tolerances are needed.

# 1. Introduction

Due to increasing global energy consumption, significant amounts of emissions are discharged into the environment [1]. Renewable energy sources are considered appropriate solutions to reduce emissions and replace conventional energy sources. Authorities are enforcing regulations to facilitate this shift. For example, the EU has set a target to secure 32% of the energy demand being provided by renewable energy sources by the year 2030 [2]. Wind energy is one of the major renewable energies that has gained momentum in recent years. Global wind turbine installations have increased capacity from 54.9 GW to 93 GW from 2016 to 2020 [3]. Offshore wind turbines (OWTs) have the relative advantages of higher wind velocity, lower surface roughness, lower wind shear, and lower turbulence intensities than onshore sites [4,5]. Among them, floating OWTs benefit from the availability of more installation areas for development and less visibility from the shore than bottom-fixed OWTs [6].

The average size of the OWTs installed in Europe increased from 3 MW in 2010 to 8 MW in 2020 [7], which expresses the need for suitable installation solutions to justify the market demand for larger turbines. The installation of floating wind turbines

E-mail addresses: behfar.ataei@ntnu.no (B. Ataei), shuai.yuan@ntnu.no (S. Yuan), zhengru.ren@sz.tsinghua.edu.cn (Z. Ren), karl.h.halse@ntnu.no (K.H. Halse).

Corresponding author.

has challenges such as increasing OWT sizes, higher installation expenses, and technical complexities. A wind turbine consists of components such as blades, hub, nacelle, tower, and substructure. They can be installed piecewise or as a single preassembled unit.

Most early research focused on the installation of OWTs by components [8]. Single blade installation of offshore wind turbines can be performed using fixed and different floating installation vessels [9,10]. The installation operation can be modeled using rigid multibody dynamics [11,12]. Blade root impact is considered a limiting factor in such operations [13] which can be mitigated using a passive tuned mass damper system [14].

Installation of the OWT as a single unit requires an installation vessel with a higher lifting capacity than piecewise installation. However, this is expected to shorten the duration of offshore operations. Multiple efforts are made to address the challenges faced during the OWT installation as a single unit. A specialized catamaran equipped with sliding grippers is a solution that constrains the motion of the installation vessel and the preinstalled substructure [15]. Windlifter is a concept introduced by Ulstein company that allows single-phase installation of an OWT unit using a specialized unit attached to the aft of the vessel [16]. In another effort, a floating dock can be used for the installation that protects the installation site from the environment [17].

Offshore heavy lift simulations are primarily performed based on rigid multibody dynamics [18,19], where the flexibility of the elements is neglected. However, to mitigate the limitation, improve simulation fidelity, and implement structure flexibility, the finite element method (FEM) is utilized to perform flexible multibody dynamics. This approach has been applied in multiple marine applications, for example, the influence of underwater current on mooring lines and risers [20,21], large-scale steel-concrete immersed tunnels [22,23], and ship-ice interaction for polar ships [24]. Implementing crane structure flexibility in conventional heavy lifting operations was found to influence the response of the payload and the installation vessel [25]. Furthermore, wind energy converters' connection to the floating structures was modeled using the FEM [26], and the fatigue life of the connection nodes was concluded to be critical. Finally, flexible multibody dynamics were utilized to design wind turbine components such as gearboxes and blades [27,28] in addition to the in-place performance of an operational OWT [29].

Recent research performed by the center for research-based innovation, marine operations in virtual environments (SFI MOVE), has yielded a low-height lifting mechanism to install the fully assembled wind turbine on top of the preinstalled substructure [30]. Initially, mechanical grippers between the installation vessel and substructure were introduced to minimize the relative motion between the OWT and the substructure [15]. It was concluded that stiff mechanical coupling between the floating bodies results in very large forces that make the operation unfeasible. Therefore, mechanical grippers were replaced with wires. In this approach, the OWT is lifted by the wires from the bottom and stabilized from higher elevations. These wires are connected to hydraulic winches that actively control the position and alignment of the OWT. Modeling and hydrodynamic analysis of this system was performed to prove the feasibility of the concept [31,32]. In addition, active control strategies using inverse dynamics and range-based localization were utilized to reduce the relative motion during the mating phase [33,34].

In the present paper, the primary motivation is to distinguish the governing components in system dynamics and assess the suitability of flexible multibody simulation compared to rigid multibody analysis. The relative motion between the hanging OWT and the floating spar buoy substructure in the SFI-MOVE concept is quantified. Furthermore, the influence of crane structure flexibility on the dynamic response of the low-height lifting mechanism is investigated.

The paper is organized as follows. The idea of the low-height lifting mechanism is introduced in Section 2. Section 3 focuses on the theoretical background of hydrodynamics and the FEM. The catamaran vessel, lifting arrangement, and OWT are assembled in the SIMA simulation environment [35], and the analysis setup is explained. Simulations are performed for various environmental conditions, and the results are presented in Section 4. Finally, Section 5 concludes the research and provides recommendations for future work.

# 2. Low-height lifting mechanism concept

# 2.1. System description

The proposed SFI-MOVE concept consists of four structures: an installation catamaran vessel, a preinstalled floating substructure (spar buoy), a wind turbine, and a low-height lifting mechanism; see Fig. 1(a). Within this concept, floating substructures are transported to the desired location and connected to the preinstalled mooring lines. The catamaran vessel equipped with the low-height lifting mechanism enables the loadout of multiple preassembled OWT units, transport to the installation site, and lifting operation execution. The low-height lifting mechanism includes two sets of 3D frame structures, a collar, several lifting and stabilizing wires, and corresponding hydraulic winches and controllers. In conventional lifting operations (see Fig. 1(d)), the crane tip reaches the payload top to lift the object, while the payload is lifted from the bottom by frame structures in low-height lifting. Hence, the proposed low-height lifting mechanism reduces the supporting structures' height and the sensitivity to the payload's dimension.

The low-height lifting mechanism can be located on the aft or side of the vessel:

• Aft positioning of the lifting mechanism can be performed by locating the structure around the vessel's centerline and inserting an opening on the vessel's hull (see Fig. 1(c)). The advantage of aft arrangement is easier transportation of the OWT units along the vessel and less complexity in the final lifting and mating operation. In addition, aft positioning reduces the possibility of a clash between the hanging tower and the installation mechanism in the following seas.

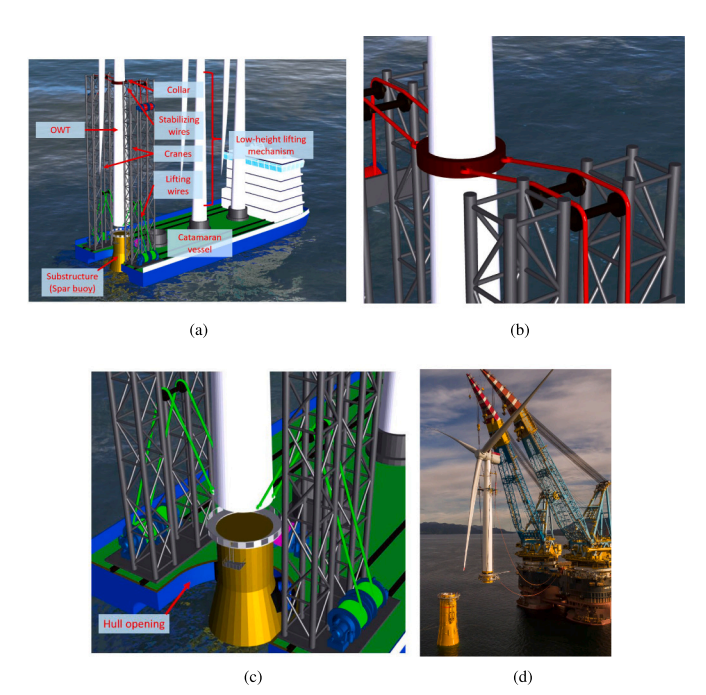


Fig. 1. SFI-MOVE concept and conventional OWT lifting operation: (a) SFI-MOVE OWT installation concept, (b) SFI-MOVE concept: Stabilizing wires connection to collar, (c) SFI-MOVE concept: Lifting wires connection to OWT, and (d) Hywind scotland OWT lifting operation using Saipem 7000 crane vessel [36].

• Side installation benefits from reduced pitch-induced vertical motion. This arrangement does not require deck opening but necessitates extra structural elements working as movable jibs, which moves OWTs from the vessel's centerline to the top of the substructure at the side. Additionally, the side operation is more sensitive to the vessel roll motion as extra weight is inserted to the vessel's side, resulting in moving the center of gravity to the side. Furthermore, this requires the insertion of counterweights and the implementation of anti-roll mechanisms such as anti-roll tanks.

This paper focuses on the single lifting operation of the preassembled wind turbine from the aft of the catamaran vessel, emphasizing the structural aspects of the lifting cranes.

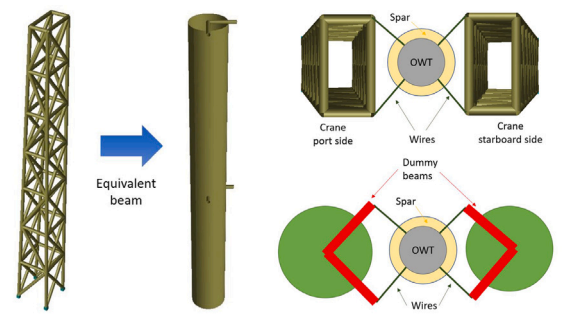
Lifting and stabilizing are performed using two wire groups. Four lifting cables are connected to the bottom of the OWT, carrying the major part of the OWT's weight and reducing the OWT bottom longitudinal and vertical displacements using multi-degree-of-freedom (MDOF) controllers (see Fig. 1(c)). Vertical alignment between the OWT and substructure is controlled by using four stabilizing cables connected to higher elevations of the OWT. These cables are connected to the collar on one side and the top of the lifting mechanism on the other side (see Fig. 1(b)). The collar is a ring structure located around the OWT tower. This structure can freely move in the vertical direction (transition in the Z-direction) while limiting the OWT horizontal motions (X- and Y-directions). The combination of the lifting and stabilizing wires reduces the relative displacement between the OWT bottom and substructure top and controls the vertical alignment between the two bodies. Each wire is connected to a hydraulic winch that controls the wire length using a controller.

This concept is advantageous due to the small installation vessel size, multiple-OWT installation with a single load-out, relatively smaller crane size, and less sensitivity toward growing OWT sizes.

# 2.2. Installation scenario

The entire installation process can be divided into the following steps:

- Step 1 Foundation preparation: The substructure is transported to the installation site and connected to the preinstalled mooring lines.
- · Step 2 Preassembly: OWT components are transferred to the yard and preassembled as a single unit.
- Step 3 Transportation: Several preassembled OWT units are loaded out onto the catamaran installation vessel. The installation vessel transports the OWT units to the installation site.
- Step 4 Positioning: The vessel approaches the preinstalled substructure and activates the dynamic positioning system to control the relative distance between the vessel and the substructure.
- Step 5 Preparing: The selected OWT is moved along the vessel's centerline to the aft using the onboard sliding system on the deck. Wires are connected to the OWT, lifting mechanism, and collar.



(a) Structural simplification proce-(b) Top: Plan view of the 3D frame structure. ture and wire connection nodes;

Bottom: Plan view of the equivalent crane structure, dummy beams and wire connection nodes.

Fig. 2. Crane structure simplification procedure and plan view of connections to the OWT.

- Step 6 Lifting: The OWT is lifted from the vessel and moved above the substructure location.
- Step 7 Mating: The OWT is lifted on top of the substructure, and mating is performed. Winches and controllers are activated to compensate for the relative motion between the OWT bottom and substructure top.
- Step 8: The vessel is moved to install the next OWT, and Steps 4-7 are repeated.

It is assumed that all the system components operate in ideal conditions throughout all phases of the installation operation. Therefore the failure of system components is not investigated here. In this paper, we focus on the mating operation (Step 7) of the installation process.

#### 3. System modeling

According to the DNV-GL regulations [37], if the weight of the lifted object reaches a specific ratio (normally 1–2%) of the vessel displacement weight, the lifting operation is considered heavy lifting. The mentioned ratio is 7% in the present research; hence, the proposed system should be analyzed as a heavy-lifting problem. Regulations demand to perform coupled simulation, i.e., the payload dynamics (here, the OWT), crane, and installation vessel influence each other and must be considered. Furthermore, this study assumes no mechanical coupling between the spar foundation and catamaran vessel.

The structural deflections of the catamaran vessel, OWT, collar, and spar buoy are relatively smaller than the motions produced by hydrodynamics or system dynamics. Therefore, these bodies are assumed to have rigid behavior. The catamaran vessel, spar buoy, and OWT are modeled as rigid bodies in the Simo module of the SIMA workbench developed by SINTEF Ocean. Wires are modeled using springs and dampers with axial tension stiffness and without compression stiffness. To consider the effect of the structural stiffness of the lifting mechanism on the relative motion between the spar top and OWT bottom, the low-height lifting mechanism is modeled using the finite element method and beam elements. Riflex is a module of the SIMA workbench developed for the finite element analysis of slender marine structures and is utilized in simulations.

The low-height lifting mechanism holds the hanging OWT from a location lower than its center of gravity (COG), resulting in unstable inverted pendulum behavior. Hence, it is necessary to use a controller to stabilize such a system. However, controllers have major effects on the system dynamics, making the current investigation cumbersome. Therefore, the controllers are deactivated in this investigation, and the height of the lifting mechanism and wire connection nodes are increased to eliminate the inverted pendulum motions.

Model simplification is necessary to understand the system dynamics and determine the nontrivial influencing factors in such a complicated setup. Efforts have been made to simplify the model. The low-height lifting mechanism consists of two cranes designed as 3D frame structures. These structures are designed to resist the self-weight, environmental loads, and excitation enforced by the catamaran vessel, OWT, wires, and winches. However, in the coupled flexible multibody analysis, detailed structure modeling adds complexities to the model and difficulties in numerical convergence. Therefore, the complex frame structures are replaced by beams with equivalent cross-section properties along the length; see Fig. 2(a). The replacement procedure can be implemented using three similarity conditions: bending stiffness, eigenfrequency, and mode shapes. Since the governing criterion for OWT installation is the relative displacement between the OWT bottom and spar top, the lateral displacement of the crane structure is selected as the criterion. Within the replacement procedure, excitation forces are applied to the 3D structure, and the lateral displacement of the structures is calculated. The simplified beam is focused on having the same displacement values by modifying the bending stiffness of the beam. The detailed design of the 3D crane structure and its influence on the overall system performance will be published in future research. The frame structure provides connection joints for wires (see Fig. 2(b)); however, a circular equivalent beam cannot provide such locations. Dummy beams are utilized to provide connection points for the wire elements. These dummy beams are connected to the crane structures on one side and the wires on the other side.

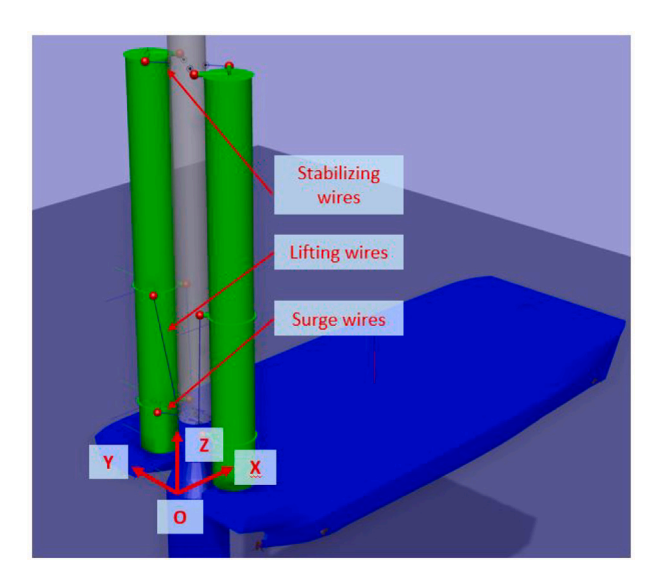


Fig. 3. Simplified system model in SIMA.

**Table 1**Main properties of spar buoy substructure.

Parameter	Unit	Value
Diameter at the top	m	9.5
Diameter at the waterline	m	14
Draft	m	70
Displacement mass	tonnes	11045
Vertical position of the COG	m	-40
Vertical position of the center of buoyancy	m	-35
Vertical position of the fairlead	m	-15
Initial position of the reference point	m	(0,0,0)

To further simplify, the collar is removed, and the stabilizing wires are directly connected to the OWT. Furthermore, four bottom surge wires are added to the bottom of the OWT to eliminate the in-plane motions (XY Plane) in addition to the lifting and stabilizing wires. Ultimately, all the mentioned components are assembled to perform system modeling. An overview of the simplified system model is presented in Fig. 3.

Coordinate systems are needed to define the body's location, orientation, and response. These coordinate systems consist of global and body-fixed coordinate systems that follow the right-hand rule. The origin O of the global coordinate system is located at the floating spar initial centroid position at the water surface level; see Fig. 3. The global X-axis is pointed toward the north, the global Y-axis is toward the west, and the global Z-axis is set upward. Body-fixed coordinate systems are considered parallel to the global coordinate system with the origin located at the reference point of each individual body. The floating object (catamaran and spar) rotations about the X-, Y- and Z-axes are defined as roll  $(\phi)$ , pitch  $(\theta)$  and yaw  $(\psi)$ , respectively. All of the responses in the present article are given in the global coordinate system; therefore, presenting the body-fixed coordinate systems is unnecessary.

#### 3.1. Spar buoy

The Hywind concept introduced by Equinor utilizes a spar buoy as the OWT substructure [38]. This concept benefits from higher hydrostatic stability, small waterplane area, and suitability for deeper operational regions and harsh marine environments such as the North Sea [39]. Stationkeeping of the spar buoy is achieved using three distributed anchor lines with an interval of 120°. The spar's reference point is located at the center of the spar at the waterline level. Slender elements are added to the rigid spar model to consider the viscous effects. The drag forces on slender elements are estimated using the Morison equation [40]. The main properties of the Hywind spar buoy before mating are presented in Table 1.

# 3.2. Catamaran vessel

In conventional wind turbine projects, such as Hywind Scotland [41], very large heavy lift vessels were used to perform the lifting operations from the top. Implementing concepts such as the low-height lifting mechanism allows the utilization of smaller vessels with smaller crane sizes than earlier projects. Compared to a monohull vessel, a catamaran is beneficial due to its larger waterplane area, increased dead weight, and improved hydrostatic stability. The catamaran's reference point is located at the vessel's center of

**Table 2**Main properties of the catamaran installation vessel.

Parameter	Unit	Value
Length overall	m	144
Breadth molded	m	60
Spacing between mono-hulls at waterline	m	38
Draft	m	8
Displacement mass	tonnes	18503
Vertical center of gravity above baseline	m	28.6
Transverse metacentric height	m	66.4
Initial position of reference point	m	(63,0,0)

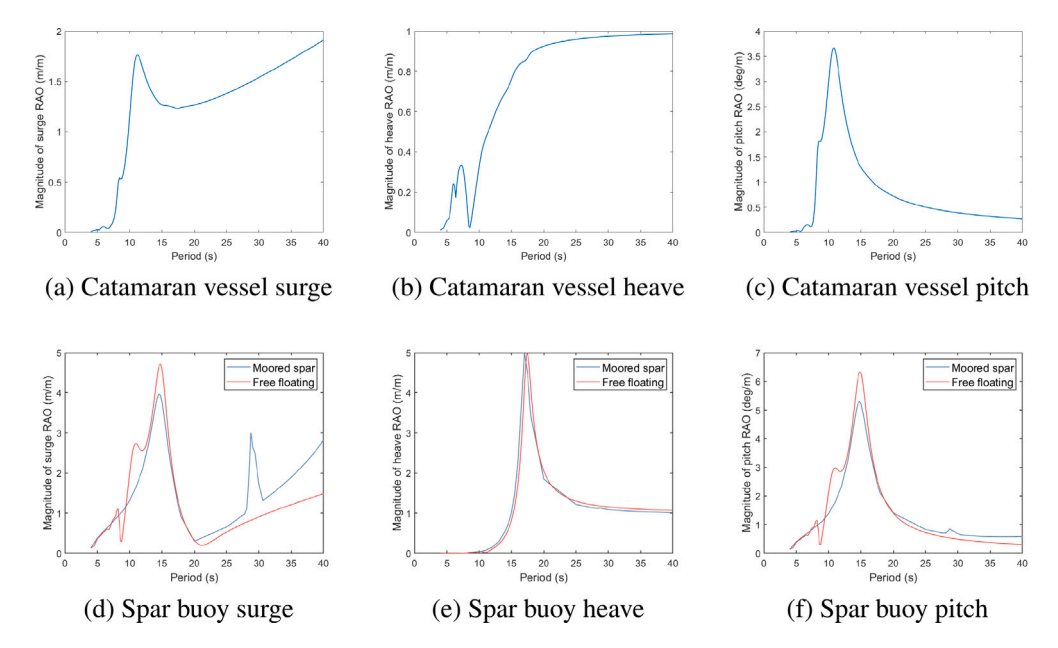


**Fig. 4.** Catamaran vessel and spar buoy surge, heave, and pitch motion RAOs at  $\beta = 0^{\circ}$ .

flotation at the waterline level. A dynamic positioning (DP) system is implemented for the catamaran vessel's stationkeeping. It is assumed that the DP system has optimum behavior, and the details of this system are beyond the scope of this paper. The principle parameters of the catamaran vessel are listed in Table 2.

The wave-induced motions are simulated using response amplitude operators (RAOs). The potential theory cannot accurately estimate the viscous effects; therefore, 3% percent roll damping is added to the catamaran vessel to consider the viscous effects. Utilizing a SWATH as an alternative installation vessel and the influence of second-order wave forces on the catamaran vessel is presented in [42]. Hydrodynamic coupling between the catamaran installation vessel and spar buoy is neglected since only some minor differences arise [43]. Surge, heave, and pitch RAOs of the free-floating catamaran vessel as well as free-floating and moored spars with wave direction  $\beta = 0^{\circ}$  are presented in Fig. 4.

Motion RAOs (Fig. 4) are presented for illustration purposes only, and force RAOs are used in the equations of motion. Note that anchoring the spar buoy with mooring lines influences the motion characteristics of the floating object. Therefore, the hydrodynamic behavior of the freely floating spar buoy is estimated in the frequency domain, and mooring lines are added as nonlinear springs within the time-domain simulation.

A comparison between the free-floating spar buoy and moored structure (see Figs. 4(d)–(f)) shows that the addition of mooring lines reduced the spar responses around the peaks in surge and pitch degrees of freedom (DOFs). This is due to the extra hydrodynamic damping added by the Morison loading on the mooring lines. The moored structure has higher surge and pitch responses in higher periods. The second peak is observed at approximately 30 s in surge and pitch caused by the mooring lines. The heave response of the spar is identical between the free-floating and moored spar buoys.

### 3.3. Wind turbine

The Technical University of Denmark 10 megawatt (MW) reference turbine [44] is used hereafter as the OWT, and the main properties of this turbine are presented in Table 3. The OWT reference point is located at the bottom of the OWT tower in the centroid. Wind turbine deflections are less critical in the present project and assumed to be rigid.

Table 3
Main properties of the DTU 10 MW offshore wind turbine.

Parameter	Unit	Value
Rated power	MW	10
Number of blades	_	3
Rotor diameter	m	178.3
Hub diameter	m	5.6
Hub height	m	119
Rotor mass	kg	227,962
Nacelle mass	kg	446,036
Tower mass	kg	628,442
Initial position of the reference point	m	(20,0,0)

#### 3.4. Wires

Three groups of wires are used in the system:

- 1. The OWT is lifted using four lifting wires, where the weight is carried. These wires are connected between the bottom of the OWT and the middle of the lifting cranes (Z = 50 m).
- 2. Stabilizing wires consist of four wires connecting the top of the lifting cranes (Z = 105 m) to the OWT and eliminating the rotation of the OWT.
- 3. Bottom surge wires are used to eliminate OWT longitudinal and lateral movement from the bottom of the OWT. These wires connect the base of the OWT to the lower heights (Z = 20 m) of the lifting cranes.

Stabilizing wires and surge wires are implemented to limit the longitudinal and lateral motions of the OWT. The locations of different wires are presented in Fig. 3.

Wires are modeled as simple wire coupling in SIMA software, which consists of tension-only elements. Pretension forces can be implemented to eliminate the slack behavior of the wires. For systems with small displacements, relatively smaller pretension forces are needed. However, in the case of large displacements, high pretension forces are required to eliminate slack behavior. Utilizing large pretension forces demands powerful winches to provide tension and results in excessive loads on structural components that make it impractical. In the current research, large displacements are expected; hence, it is assumed that wires are not pretensioned and can act as slack elements. Wires are modeled as nonlinear springs given by

$$T = \max\{ \Delta l \cdot \frac{EA}{l}, 0 \}, \tag{1}$$

where *T* is the wire tension,  $\Delta l$  is the elongation, *l* is the initial length, *E* is the modulus of elasticity, and *A* is the cross-section area. Hereafter, we use values of  $EA = 7.7 \cdot 10^8 \ N$  and a damping ratio of 1%.

#### 3.5. Rigid and flexible cranes

To evaluate the effect of structural flexibility, two different models are developed. An overview of these two models is presented in Fig. 5. In both models, the hydrodynamic properties of the vessel are estimated with the fully loaded draft (also called the heavy ship condition). In contrast, the vessel's mass matrix must be modified within the time-domain simulation. Heavy ship condition is estimated as the summation of catamaran lightweight, three 10 MW OWT units, and two sets of lifting cranes.

- Model 1: Cranes are assumed to be rigid and inherent parts of the vessel without deformation. One OWT hangs from the wires; therefore, this item must be subtracted from the vessel's global mass matrix. This approach assures that the system's total mass is kept constant and in accordance with the heavy ship condition.
- Model 2: Cranes are flexible with deformation and modeled as beam elements. The hanging OWT is modeled as a rigid body. Therefore, these items must be eliminated from the vessel mass matrix to prevent duplication in the simulations.

# 3.5.1. Model 1: Rigid multibody model

Regarding rigid cranes, wire connection nodes follow the vessel motions and carry the OWT weight. Three rigid bodies (including the catamaran vessel, spar buoy, and OWT) are modeled using 6DOF rigid body kinetics. The governing time-domain equation of motion for the rigid multibody [45] is given by

$$M\ddot{\eta} + C\dot{\eta} + D_1\dot{\eta} + D_2f(\dot{\eta}) + K(\eta)\eta = q(t, \eta, \dot{\eta}), \tag{2}$$

where  $\eta$ ,  $\dot{\eta}$  and  $\ddot{\eta}$  are the position, velocity, and acceleration vectors, respectively; M is the frequency-dependent mass matrix (including the added mass); C is the frequency-dependent potential damping matrix;  $D_1$  is the linear damping matrix;  $D_2$  is the quadratic damping matrix; f is a vector function; K is the hydrostatic stiffness matrix of the floating objects and mooring lines for the spar buoy; and q is the sum of environment-induced excitation forces and thruster forces using the DP system. The Runge Kutta numerical method with a 0.01 s time step is utilized to solve the equation.

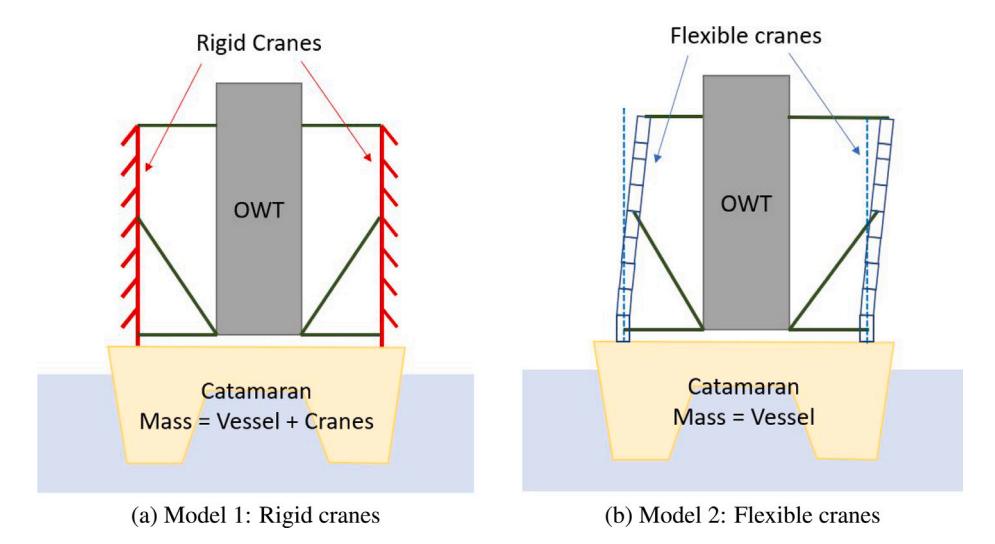


Fig. 5. Overview of the two models.

#### 3.5.2. Model 2: Finite element modeling of lifting cranes

The FEM is utilized to simulate the effect of the lifting mechanism structure flexibility. The structure is divided into a number of elements that are connected via nodes. This allows the transfer of internal forces and external excitation within the structure.

Beam elements are considered suitable for modeling crane structures because their length is relatively larger than the cross-section dimensions, and stresses along them are more important. Each three-dimensional (3D) beam element has 6 DOFs, consisting of three transitions and three rotations along the coordinate axis. Crane structures are modeled using beam elements with axisymmetric cross-sections. These beam elements have axial, bending, shear, and torsional stiffness properties. The cranes' reference points are located on the installation vessel deck level at the center of each crane. Dummy beams are modeled using beam elements with very large stiffness and zero damping.

This problem can be solved in static and dynamic analyses. Static analysis is essential to find static equilibrium, which is used as the initial condition in the dynamic analysis. The system reaches static equilibrium when the structure's internal reaction forces  $R^S(r)$  and external forces  $R^E(r)$  are in balance, i.e.,  $R^S(r) = R^E(r)$ . The Newton–Raphson iterative procedure is implemented for the solution of the non-linear static analysis.

The flexible multibody dynamic time-domain equation [46] is given by

$$R^{I}(r, \ddot{r}, t) + R^{D}(r, \dot{r}, t) + R^{S}(r, t) = R^{E}(r, \dot{r}, t), \tag{3}$$

where  $r, \dot{r}, \ddot{r}$  are structural displacement, velocity and acceleration vectors,  $R^I$  is the inertia force vector, and  $R^D$  is the damping force vector. The dynamic equation of motion is solved in the time domain using the Newmark- $\beta$  time stepping method with values of  $\beta = 0.25$  and  $\gamma = 0.5$ .

The equivalent cranes are composed of three beams with lengths of 12.1 m, 30 m, and 55 m. The horizontal planes defining these beam lengths are the vessel deck (Z = 7.9 m), surge wires (Z = 20 m), lifting wires (Z = 50 m), and stabilizing wires (Z = 105 m). A mesh sensitivity analysis is performed to investigate the influence of the element length (EL) on the finite element systems response. The beam ELs are reduced from the initial size of 12.1 m, which is the largest element size possible for the bottom beam, and are reduced to the minimum value of 0.12 m for each beam. An analysis is carried out with nine ELs of 12.1 m, 6.05 m, 4.03 m, 3.03 m, 2.42 m, 2.02 m, 1.21 m, 0.24 m, and 0.12 m. Time histories of the global X-direction response top of the crane node located at the port side for different beam ELs are presented in Fig. 6. The 100-second simulation results for  $H_s = 1$  m and  $T_p = 10$  s are extracted and shown.

The results show different beam element lengths have similar X-direction transitions. Furthermore, the same trend is observed for the crane structure transitions in the other directions and environmental conditions. All the different element lengths provide consistent responses, and having too small elements does not contribute to the computational accuracy but increases the computational costs. Here, the element length is selected as 2 m, providing sufficient computational efficiency. In addition, the equivalent crane structure can be compared with a cantilever beam. The analytical results of the cantilever beam for lateral deflection and natural periods match the numerical results generated in Sima.

Global Rayleigh damping C is defined as a linear combination of mass  $M_i$  and stiffness matrices  $K_i$ ,  $C = \alpha_1 M_i + \alpha_2 K_i$ , where  $\alpha_1$ ,  $\alpha_2$  are mass- and stiffness-proportional damping coefficients, respectively. Orthogonality of mode shapes allows to define modal damping  $\lambda_i$  as the function of damping coefficients, i.e.,  $\lambda_i = \frac{1}{2} \left[ \frac{\alpha_1}{\omega_i} + \alpha_2 \omega_i \right]$ , where  $\omega_i$  is the i'th eigenfrequency [46]. It is assumed that the first and second modes have damping ratios of 1%, resulting in  $\alpha_1$ = 0.0116 and  $\alpha_2$ = 0.0043. The time step is set at 0.01 s for the simulations.

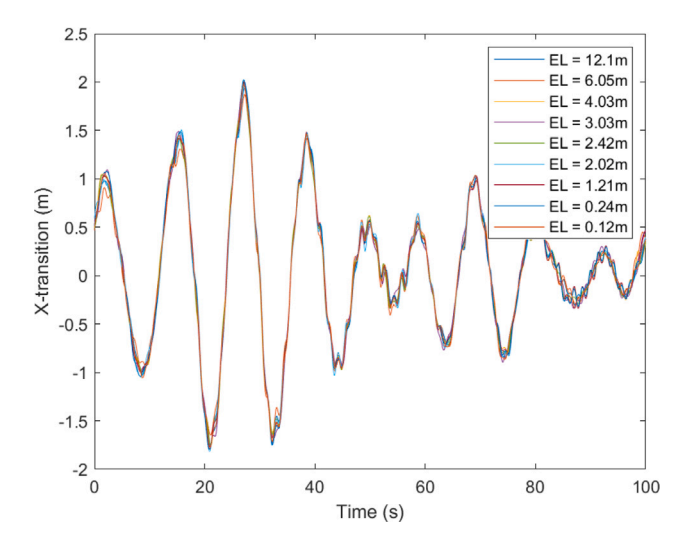


Fig. 6. Time histories of X-direction transition response of top of the crane at port side for varying beam element lengths ( $H_x = 1 \text{ m}$  and  $T_n = 10 \text{ s}$ ).

#### 3.6. Eigenvalue analysis

Resonance can occur when the natural periods of the structure match the environmental excitation periods. To prevent this phenomenon, it is beneficial to design the system so that the natural periods of the structures stay far away from the dominant frequency content of the environmental loading. The uncoupled and undamped natural periods (T) of the catamaran vessel and spar are calculated using [40]

$$T_{ni} = 2\pi \sqrt{(\frac{m_{ii} + a_{ii}}{c_{ii}})},$$
 (4)

where subscript n is the floating object's abbreviation (c for catamaran and s for spar), subscript i is the degree of freedom, m is the mass, a is the added mass, and c is the restoring force. For the catamaran vessel, c is rooted in hydrostatic stiffness. For the spar, it comes from mooring lines in addition to the hydrostatic stiffness. The catamaran vessel has the heave and pitch natural periods of  $T_{c3} = 6.76$  s and  $T_{c5} = 9.79$  s. The spar buoy has heave and pitch natural periods of  $T_{c3} = 17.02$  s and  $T_{c5} = 13.62$  s, respectively. The mentioned heave and pitch natural periods are close to the peaks of uncoupled RAOs presented in Fig. 4.

Eigenvalue analysis of a standalone lifting crane is assembled and performed using the Riflex finite element tool; see Fig. 7. Eigenfrequencies and vectors can be found using the equation

$$[K_e - \omega_e^2(M_e + A_e)]\phi_e = 0,$$
 (5)

where  $K_e$  is the stiffness matrix,  $\omega_e$  is the natural frequencies,  $M_e$  is the mass matrix,  $A_e$  is the hydrodynamic added mass (here zero), and  $\phi_e$  are the eigenvectors.

Analysis shows that the first natural period of lifting crane structures occurs at T=1.471 s (f=0.680 Hz). The crane structure has identical stiffness in all directions due to its axisymmetric cross-section; therefore, the mode shapes can occur in all directions for a specific natural period. The second natural period takes place at T=0.254 s (f=3.930 Hz). Structural eigenvalue analysis shows that the first two vibration modes do not occur within the excitation periods enforced to the system by the wave spectrum. Higher order modes have periods less than 1 s, which are less important.

The mentioned natural periods are estimated for the moored spar buoy, catamaran vessel in the heavy ship condition, and standalone lifting crane. However, the low-height lifting mechanism influences the system's natural periods due to coupling effects. Within both models, the hanging OWT is connected to the vessel and crane using nonlinear wire elements. Lifting wires provide stiffness when they are under tension while behaving as slack in compression. This behavior introduces nonlinearities into the system, which makes coupled eigenvalue analysis impossible. Therefore, to determine the natural periods of the system, decay tests are performed using time-domain simulations. Reduction of the beam stiffness under the axial forces is considered at this stage. In this approach, a certain DOF (in model 1 and 2) is given an initial value, and then the system is allowed to vibrate until the motion vanishes. Fig. 8 presents the time histories of the catamaran vessel heave response in model 1 when the OWT reference point Z-coordination is moved from the initial position of Z = 20 m to Z = 21 m and then released. High-frequency behavior is observed in the beginning, rooted in transient responses and wire dynamics. After elimination of the transient responses, the catamaran vessel is oscillating with a period of 6.2 s, which is reduced due to hydrodynamic damping. A summary of the eigenvalue analysis is presented in Table 4.

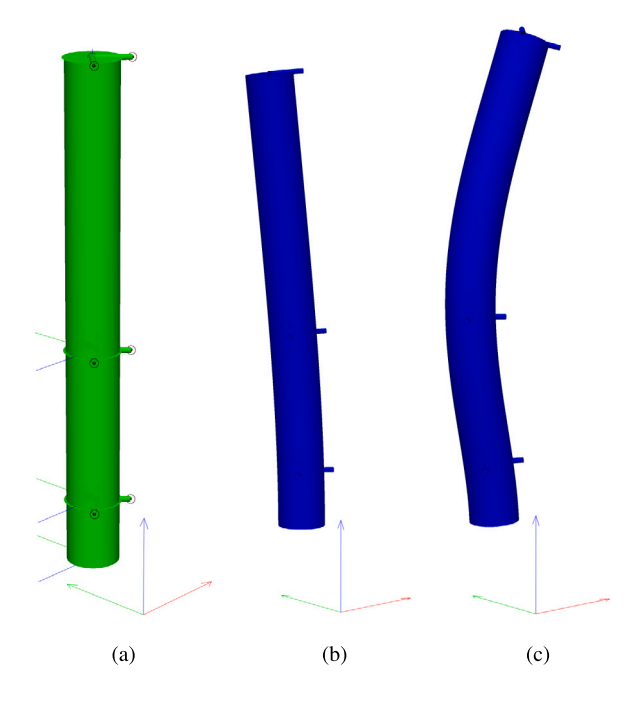


Fig. 7. Overview of a standalone crane structure and first and second mode shapes: (a) standalone lifting crane model, (b) first mode shape, and (c) second mode shape.

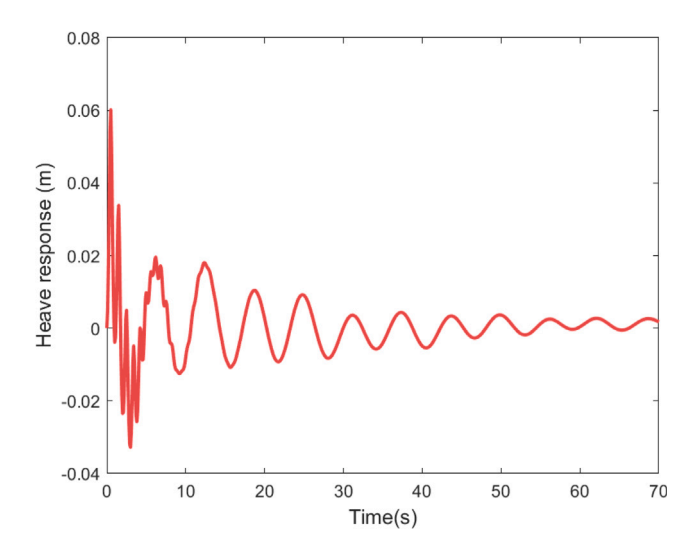


Fig. 8. Decay test of the catamaran heave DOF in model 1 (with rigid crane) when the OWT initial location is modified.

In Model 1, coupling the catamaran vessel and the OWT with the wires influences the natural periods of the catamaran vessel. The heave natural period is slightly shifted from 6.76 s to 6.2 s, and the pitch natural period has increased from 9.79 s to 12.0 s. High-frequency vibrations with periods less than 1 s are observed in the OWT response, which is rooted in the wires' stiffness.

In Model 2, the vessel has a heave natural period of 6.4 s, which is close to the original free-floating vessel heave natural period of 6.76 s. The catamaran's pitch natural period is increased from 9.79 s to 12.8 s. OWT motions are influenced by high-frequency vibrations of approximately 1 s, which are sourced in the wires and crane structure vibrations in addition to vessel motions.

Table 4
Summary of eigenvalue analysis.

Description	Natural period (s)			
	Heave	Pitch	Mode 1	Mode 2
Catamaran vessel in heavy ship conditions	6.76	9.79	_	_
Catamaran vessel with rigid cranes (Model 1)	6.20	12.00	_	-
Catamaran vessel with flexible cranes (Model 2)	6.40	12.80	-	-
Spar	17.02	13.62	-	-
Crane structure	_	_	1.47	0.25

Table 5
Overview of environmental conditions.

EC	Wave height (m)	Wave period (s)	Direction (°)
1	H = 2, 3, 4, 5, 6	T = 10	0
2	H = 2	$T = 4, 5, \dots, 17, 18, 20, 25, 30, 35, 40$	0
3	$H_s = 1, 1.5, 2, 2.5, 3$	$T_p = 10, 12$	0
4	$H_s = 1$	$T_p = 6, 7, 8, 9, 10, 11, 12, 14, 16$	0
5	$H_s = 1$	$T_p = 6, 7, 8, 9, 10, 11, 12, 14, 16$	0, 15, 30, 45, 90, 165, 180

#### 4. Simulations and results

#### 4.1. Environmental conditions

The main focus of the present research is to evaluate the effect of low-height lifting mechanism flexibility on the installation of an OWT unit under the influence of environmental excitation. To reduce the complexity of the problem, the effects of the wind and current are disregarded in the simulations, and the main focus is on the waves. It is assumed that the installation site has a water depth of 130 m.

A summary of five sets of environmental conditions (ECs) with regular and irregular waves is presented in Table 5. Here, H stands for the regular wave height, T is the regular wave period, and  $H_s$  are the significant wave height and the peak period for irregular waves, respectively. In EC1, the regular wave period is set at a constant value of T=10 s, and the wave height increases from 2 m to 6 m. In EC2, the regular wave height is set to H=2 m, and the period varies from 4 to 40 s. Irregular waves on EC3, EC4, and EC5 are generated using the JONSWAP spectrum with a peakedness parameter of 3.3 [47]. In EC3, the peak period is assumed to be fixed ( $T_p=10$  and 12 s), and the significant height is varied. In EC4, the significant wave height is kept constant ( $H_s=1$  m), and the peak periods are varied. Most of the simulations are performed in the following sea orientation ( $\theta=0^{\circ}$ ), assuming long-crested waves. EC5 is performed with seven wave directions (varying from  $0^{\circ}$  to  $180^{\circ}$ ) to consider the sensitivity to wave angle.

In all ECs, the response of the catamaran reference point, spar reference point, OWT bottom (mating position), wire connection nodes on the lifting mechanism, wire forces, and relative motion between the OWT bottom and spar top are compared between the flexible and rigid structures.

For regular waves (EC1 and EC2), simulations are performed for the duration of 100 wave periods. The results from the first 90 wave periods are neglected to assure that the system is steady and avoid transient responses. The results from the last ten wave periods are averaged for the response assessment. Irregular environment case studies are performed for 3600 s after the transient response has vanished. Five random wave seeds are selected for the irregular simulations, and the results are averaged and reported for these cases. The simulations are performed on a workstation with a 3.20 GHz Xeon processor with eight cores. Each of the analyses with irregular waves took 2506 s for the flexible model to run and 321 s for the rigid model. Modeling cranes with appropriate flexibility properties provide higher fidelity analysis while increasing the computational costs substantially.

#### 4.1.1. Static analysis results

The catamaran vessel's weight and buoyancy, ballast forces, OWT weight, structural self-weight, and wire pretension forces (zero in this case) are assumed to be loads within the static simulation. The static analysis results are identical between environmental conditions since all the static forces are constant and independent of the environmental loading. We have developed two models to evaluate the effect of the flexibility of the crane structure, and the static analysis results in

**Model 1 (rigid crane):** The OWT has a displacement of 15 cm to its initial position in the Z-direction that is rooted in the elongation of the wires due to the OWT weight. The wire connection nodes do not have any deflections, as they are rigidly connected to the vessel.

Model 2 (flexible crane): It is observed that the OWT weight results in wire elongation and OWT displacement of 15 cm in the Z-direction. In this case, the top of the crane structure deflects 7 cm in the lateral direction (Y-direction). Structural deformation in the longitudinal direction (X-direction) is small, which is due to the cancellation of horizontal wire forces from aft and fore connection points. The axial stiffness of the crane structures is relatively large, which results in relatively small deflections in the vertical direction (Z-direction).

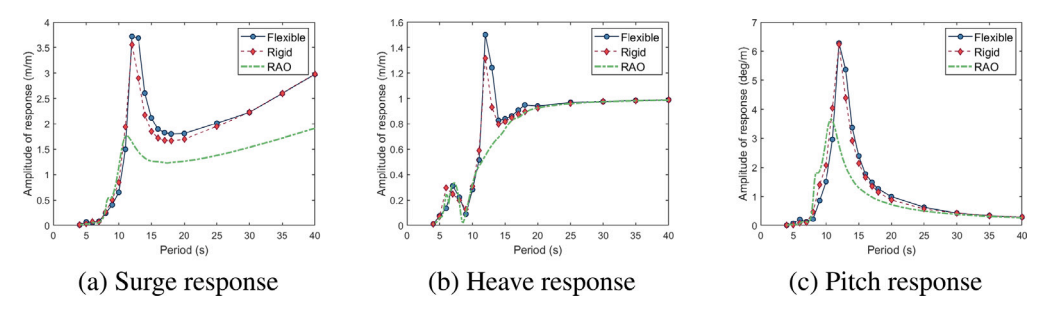


Fig. 9. Catamaran vessel response in surge, heave and pitch for EC2 and comparison with the original RAO.

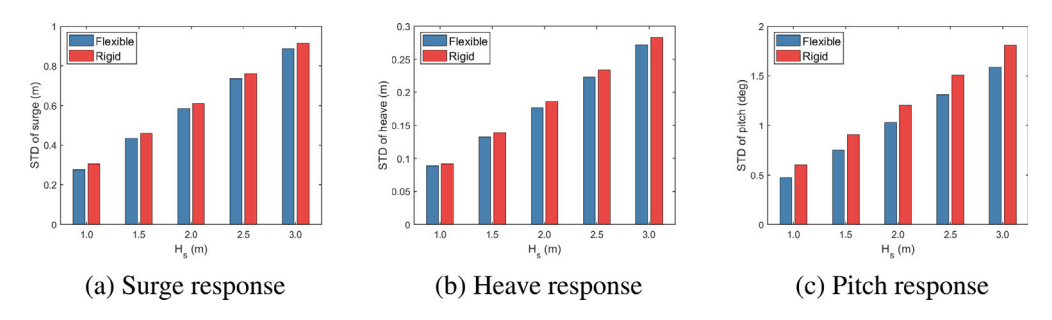


Fig. 10. Catamaran vessel response in surge, heave and pitch motions for EC3,  $T_n = 10$  s.

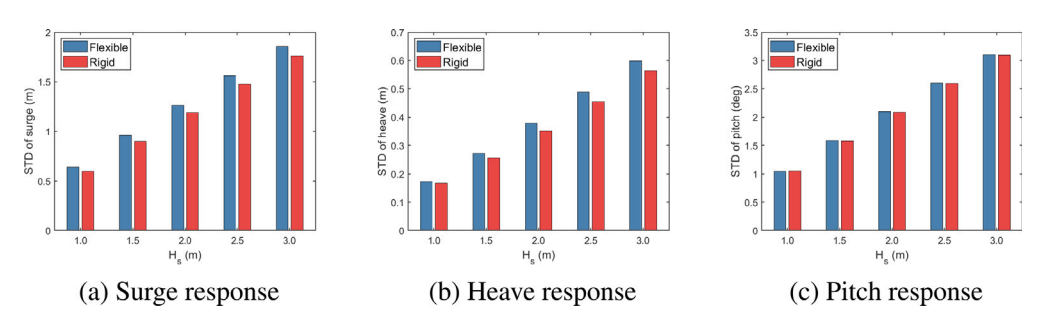


Fig. 11. Catamaran vessel response in surge, heave and pitch for EC3,  $T_n = 12$  s.

# 4.2. Catamaran vessel response

A catamaran vessel is one of the main components in the installation setup as it serves as the base for the cranes and the OWT. The response amplitudes from the time domain simulations in EC2 for the two models are compared with the vessel's original RAO and presented in Fig. 9. From Fig. 9(a), the coupling effect of the OWT and crane increases the amplitude of the vessel response in surge. In addition, it moves the peak to larger periods, from 10.6 s to 12 s. In very low and high periods of excitation (T < 8 s and T > 30 s), the catamaran vessel has identical behavior between the two models. In intermediate levels of excitation periods (8 < T < 30 s) and before the peak at 12 s, the rigid crane has a larger response amplitude, while after the peak, there is a change in this behavior.

New peaks due to heave-pitch coupling are observed for the heave response in Fig. 9(b), which was not seen in the original RAO. In addition, the catamaran vessel heave responses with flexible cranes are smaller in the range of period < 12 s and larger in the range of period > 12 s compared to rigid cranes.

From Fig. 9(c), the coupling effect increases the amplitude of the pitch response, especially around the resonant period. Furthermore, it moves the peak of the response amplitude to the higher periods. The catamaran with the rigid crane (Model 1) has a higher response for excitation periods lower than the peak, while a reverse trend is observed after the peak.

The standard deviation (STD) of the catamaran vessel's reference point in EC3 and  $T_p = 10$  and 12 s are shown in Figs. 10 and 11. These figures show that increasing the wave heights increases the vessel's response linearly. At  $T_p = 10$  s (see Fig. 10), the rigid crane has larger surge, heave, and pitch responses, while at  $T_p = 12$  s (see Fig. 11), the flexible crane enforces larger responses.

The STD of the Catamaran's vessel reference point response for EC4 is presented in Fig. 12. For the surge response (see Fig. 12(a)), in periods less than 12 s, the rigid crane has a larger response than the flexible crane, while the behavior changes after this period.

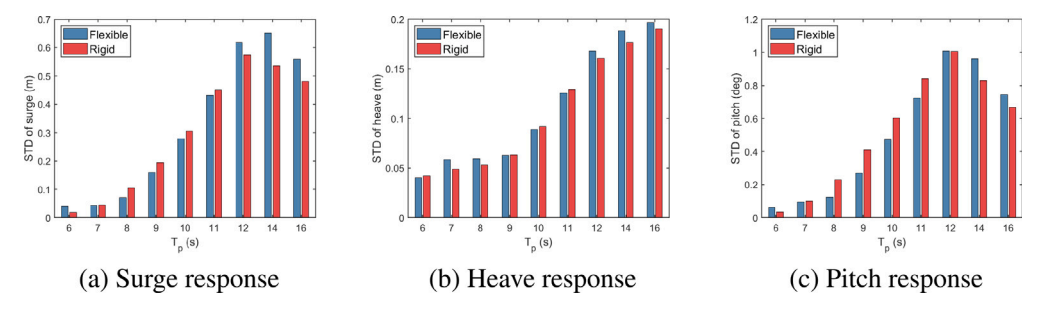
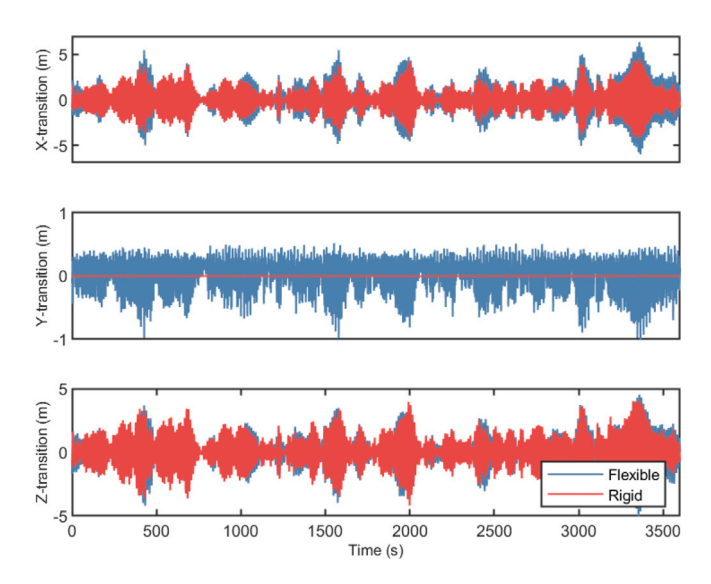


Fig. 12. Catamaran vessel response in surge, heave and pitch DOFs for EC4.



**Fig. 13.** Response of the crane top,  $(H_c = 1 \text{ m and } T_n = 12 \text{ s})$ .

The heave response (see Fig. 12(b)) shows less variation, as the STD values are relatively small. Hence, the largest difference is around natural periods for the flexible cranes. The pitch is the most significant response (see Fig. 12(c)). In periods less than 12 s, the rigid crane has a larger response, which changes after this peak.

#### 4.3. Crane structure displacements

To evaluate the effects of crane structure flexibility, the responses of the different nodes on the crane structures are calculated and compared. The motions of the crane top are of major importance, as they are expected to have the largest displacements along the beam due to their cantilever behavior. Waves are enforced in the following sea direction, and the catamaran vessel has symmetry on the X-Z plane. Therefore, there is no coupling between the catamaran's sway and roll responses with other DOFs. Hence, no displacement in the Y-direction is expected for the rigid model. However, in the flexible model, the weight of the hanging OWT results in Y-direction displacements. This effect changes the dynamic forces of the wires in the Y-direction and, as a result, produces deflections in this direction. This effect is sensitive to the wires' arrangement and the connection points (see Fig. 2(b)).

The time histories of the structural displacements for the lifting crane located at the port side and top of the structure for EC4 with  $H_s = 1$  m and  $T_p = 12$  s are presented in Fig. 13. The flexible structure has a higher deformation in the X-direction, and it shows lateral deflection within the Y-direction. The displacements in the Z-direction for the two models are similar, but the flexible model gives a slightly larger response than the rigid model. Flexible cranes have large axial stiffness that results in limited deflections in the Z-direction and similar behavior to the rigid cranes.

The top of the crane structure response amplitudes for varying wave heights (EC1) are presented in Fig. 14. This figure shows that the response amplitudes of the crane top increase linearly with the wave amplitudes. The difference between the rigid and flexible structures also increases with increasing wave amplitude. As the flexible cranes behave similarly to long slender beams, their lateral displacements are substantial. At low wave heights, the rigid crane has a slightly larger X-direction response than the flexible crane following the catamaran vessel surge motion. By increasing the wave height, the longitudinal deflection of the crane structures contributes more to the X-direction response for the flexible model. This results in a higher X-direction response for the flexible model compared to the rigid model at larger wave heights (see Fig. 14(a)). In the Y-direction (see Fig. 14(b)), the rigid cranes

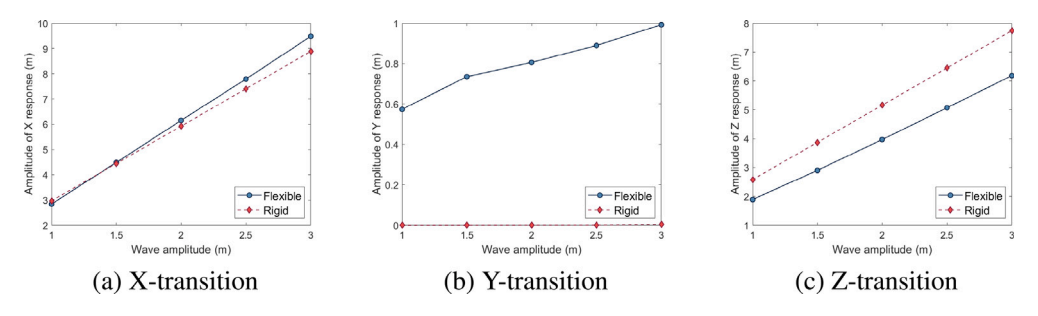


Fig. 14. Top-of-crane response in the X-, Y-, and Z-directions in EC1 (T = 10 s).

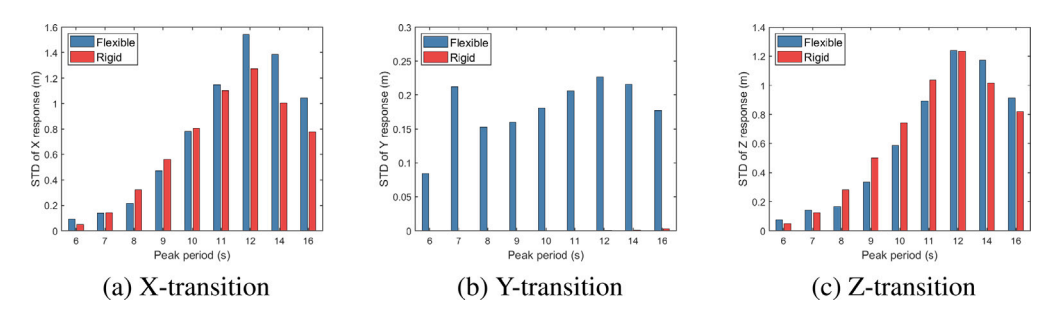


Fig. 15. STDs of crane top responses in the X-, Y- and Z-directions in EC4.

cannot reflect any response. In contrast, the flexible cranes exhibit linear behavior in the Y-direction. The response amplitude of both the rigid and flexible cranes grows linearly in the Z-direction (see Fig. 14(c)). Rigid cranes have a larger response than flexible cranes, and the difference enlarges in higher wave amplitudes following the same pattern as the catamaran vessel heave RAO at T = 10 s (see Fig. 9(b)).

Fig. 15 shows the standard deviation of the crane top responses in irregular sea states with varying peak periods (EC4). The longitudinal structural response (X-direction) is smaller for the flexible cranes before  $T_p = 10$  s and changes the behavior after this period (see Fig. 15(a)). The rigid model cannot provide any displacements in the lateral direction (Y direction; see Fig. 15(b)). The flexible structure has a peak at  $T_p = 12$  s, which is in line with the catamaran vessel pitch natural period. The peak at  $H_s = 7$  s is associated with the heave resonance of the catamaran. Fig. 15(c) illustrates the vertical responses of flexible and rigid structures. The Z-direction response is slightly smaller for the flexible structure than for the rigid crane when T < 12 s, and the reverse behavior is observed for  $T \ge 12$  s. The peak at 12 s in the Z-response is rooted in the catamaran pitch natural period.

# 4.4. Wire tensions

The time histories of lifting, stabilizing, and surge wires located in the port side and front for  $H_s = 1$  m and  $T_p = 12$  s are presented in Fig. 16. The results show that lifting wires have the same mean tension for the rigid and flexible cranes with larger fluctuations for the flexible model. Stabilizing wires face slack conditions in both models with slightly larger amplitudes of tension for the flexible model. Surge wires have slack behavior primarily for the flexible crane model, while the rigid crane model is constantly under tension. Furthermore, the flexible crane model has higher amplitude responses for surge wire tensions.

The mean and STD of the sum of the axial wire tensions for each wire group are presented in Fig. 17. The STD values are proportional to the range of variations in the wire tensions and are highlighted in this figure.

Lifting wires take care of the OWT gravitational force; therefore, the mean of the sum of these wires' tensions (see Fig. 17(a)) is approximately equal to the weight of the hanging OWT. However, the STD of the tension varies. In both rigid and flexible cranes, lifting wires' tensions increase closer to the natural periods with maximum values at  $T_p = 12$  s, which is close to the catamaran vessel's pitch natural period. The STD values for the lifting wires' tensions are larger (mean difference in STD is 26.87%) for flexible cranes than for rigid cranes.

Stabilizing wires are used to regulate the rotation of the OWT. Tensions of these wires (see Fig. 17(b)) reach maxima at the catamaran vessel's pitch natural period, where an equal mean value for the two models is observed. Using the flexible model, the STD values are relatively larger, and this difference is enlarged as the wave period approaches the peak. Stabilizing wires have lower mean values for the flexible model than the rigid cranes at lower excitation periods. The catamaran vessel pitching response is larger for the rigid model than the flexible model in the  $T_p < 12$  s range; therefore, the stabilizing wires are more severely activated compared to the flexible model.

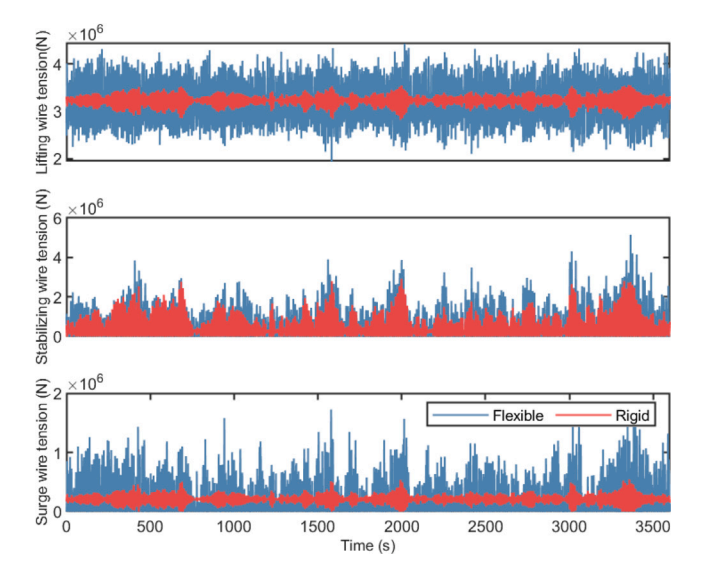


Fig. 16. An illustrative time history of lifting, stabilizing, and surge wire tensions ( $H_s = 1$  m and  $T_p = 12$  s).

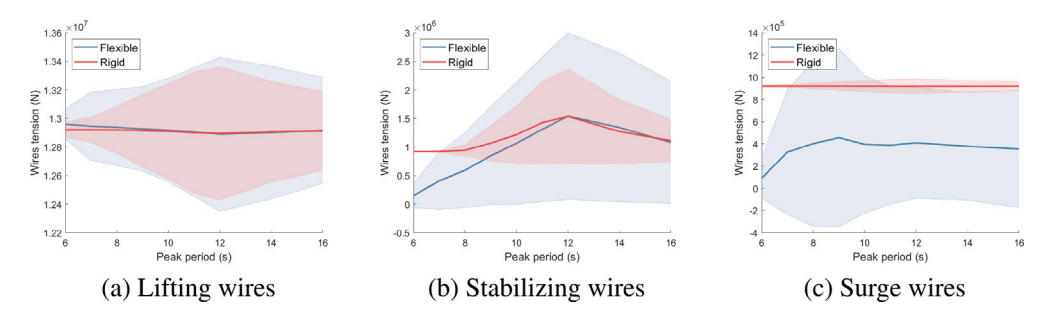


Fig. 17. Mean and range of tensions acting on the lifting, stabilizing, and surge wires with different  $T_n$  in EC4.

Surge wires are implemented to eliminate the motion of the OWT bottom. Both rigid and flexible cranes have constant mean values for different peak periods (see Fig. 17(c)), and the rigid cranes have higher mean values than the flexible cranes. Rigid cranes have a smaller STD than flexible cranes.

The amplitudes of tension on the lifting wires are on the order of  $10^4$  kN, while they are  $10^3$  kN and  $10^2$  kN for the stabilizing and surge wires, respectively. This means that the lifting wires contributed the most by carrying the weight of the OWT while stabilizing wires resisted against the OWT's lateral motions.

An investigation is performed with and without the presence of surge wires to estimate the influence of these wires on the overall system performance. The first 200 s time histories of the OWT bottom response in EC4 ( $H_s = 1$  m and  $T_p = 10$  s) are presented in Fig. 18. These results show that the presence of surge wires influences the X-direction response of the OWT reference point. The STD of the OWT bottom response is reduced to 0.107 from 0.187 for the rigid model and to 0.125 from 0.329 for the flexible model after the implementation of surge wires. However, these wires do not influence the OWT bottom Z-direction and Y-rotation responses.

# 4.5. Wind turbine motions

OWT motion is influenced by the vessel's response, cranes deflection, and wires tension. In the previous sections, the responses of the catamaran vessel and crane structures were calculated for two different crane models (rigid and flexible), and here, the OWT bottom response is studied. The time histories of OWT reference point transitions in the X- and Z-directions and rotation around the Y-direction in EC4 ( $H_s = 1$  m and  $T_p = 12$  s) are presented in Fig. 19. There is a slight difference in the X-direction response of the OWT reference point between the rigid and flexible cranes. The OWT reference point has larger displacements for the flexible crane than the rigid one. Earlier larger responses were observed for the crane structures in the X-direction (see Fig. 13). Therefore, the wires reduced the OWT response in the X-direction for the rigid and flexible cranes. The Z-direction responses of the OWT bottom

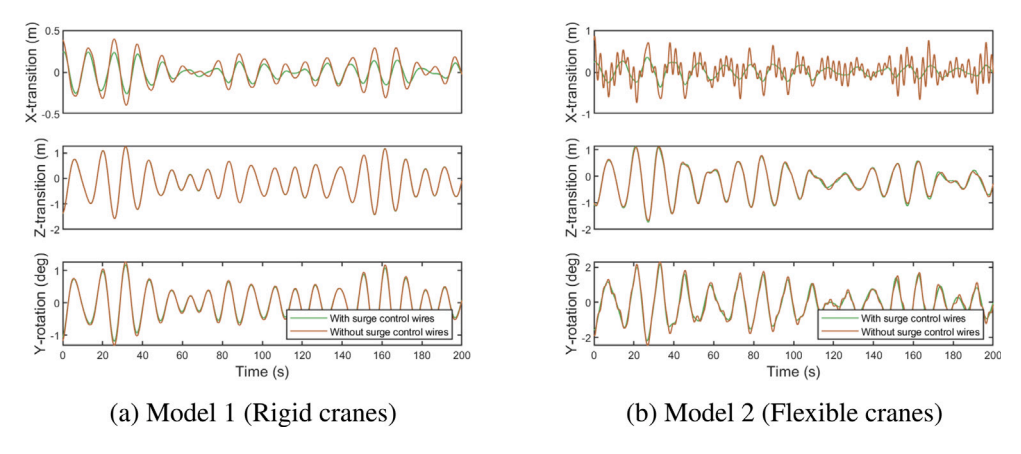


Fig. 18. Time histories of OWT reference point responses ( $H_s = 1 \text{ m}$  and  $T_p = 10 \text{ s}$ ).

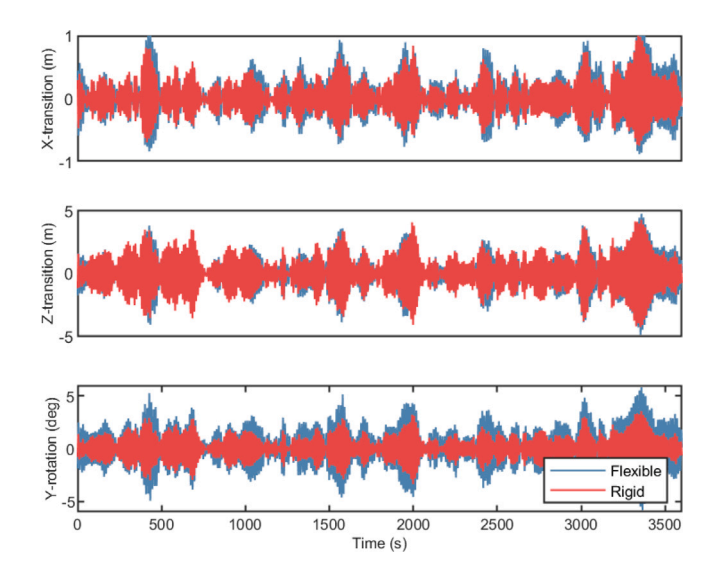


Fig. 19. OWT reference point responses ( $H_s = 1 \text{ m}$  and  $T_p = 12 \text{ s}$ ).

in the two models are close to each other, with a slightly higher response for the flexible crane than the rigid crane. In regard to the rotation around the Y-direction response, the flexible crane introduces a more significant response than the rigid model. This can be explained by the presence of structural flexural flexibility in the longitudinal and lateral directions and increased X-direction response of the crane structure top.

The response amplitudes of the OWT bottom in EC1 with a constant wave period of T=10 s and varying amplitudes are presented in Fig. 20. Increasing the wave amplitudes increases the OWT bottom response linearly in both models. The model with flexible cranes has a larger response for transition in the X-direction and rotation around the Y-axis. In contrast, the rigid crane has a higher response than the flexible crane for the transition in the Z-direction. The difference between the two models increases as the loading amplitude increases for the transition in the Z-direction and rotation around the Y-axis. However, the difference reduces for the X-direction response. For very high excitation amplitudes, the contribution of the vessel response in the OWT X-direction response becomes more significant than the contribution of the wires and cranes structural flexibility.

The response of the OWT bottom in EC4 is presented in Fig. 21. The X-direction response of the OWT bottom is larger for the model with the flexible crane compared to the rigid model in all peak periods. The pattern shows that the catamaran vessel's surge response governs the OWT bottom X-transition response (following the catamaran surge RAO). The catamaran vessel has a pitch natural period of approximately 12 s and, heave and pitch DOFs are coupled. The OWT is connected to the vessel via cranes and wires; therefore, it is expected to have peaks at this period in the Z-direction and rotation around the Y-axis responses of the OWT bottom. The OWT bottom Z-direction response is higher for the rigid cranes for periods smaller than  $T_p = 12$  s, and the behavior changes after this peak. The STD values are larger for the Z-direction transition than for the X-direction transition. Therefore, the Z-direction response is expected to contribute more to the relative motion between the OWT and spar. For the rotation around the Y-axis, the model with flexible cranes has larger rotations around the Y-axis for all peak periods.

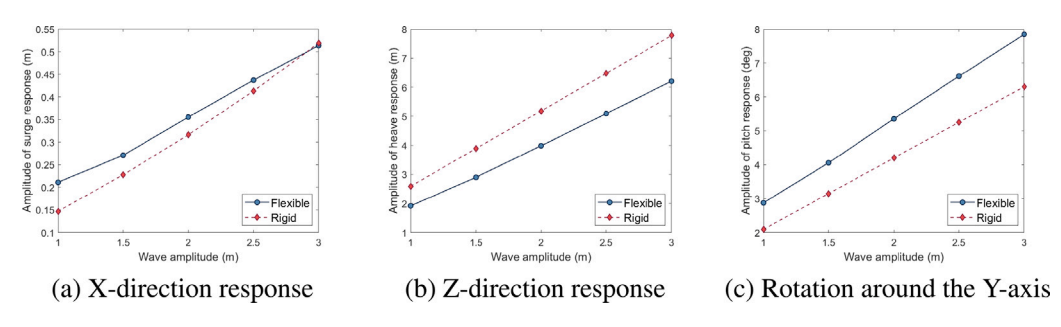


Fig. 20. OWT reference point motion in surge, heave, and pitch in EC1.

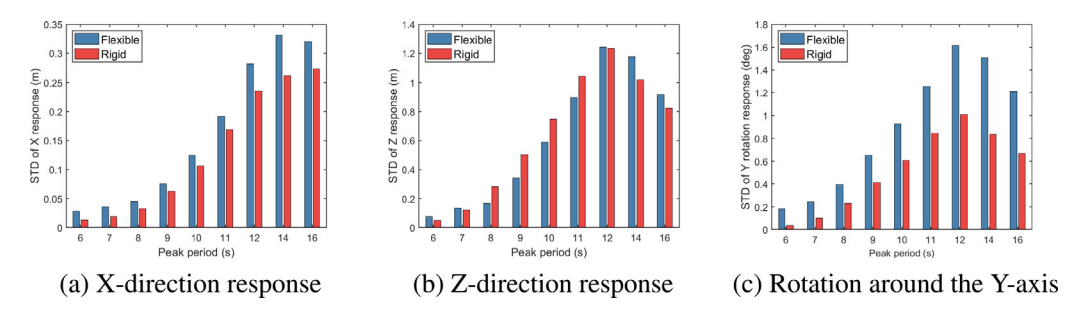


Fig. 21. OWT reference point transition in the X- and Z-directions and rotation around the Y-axis in EC4.

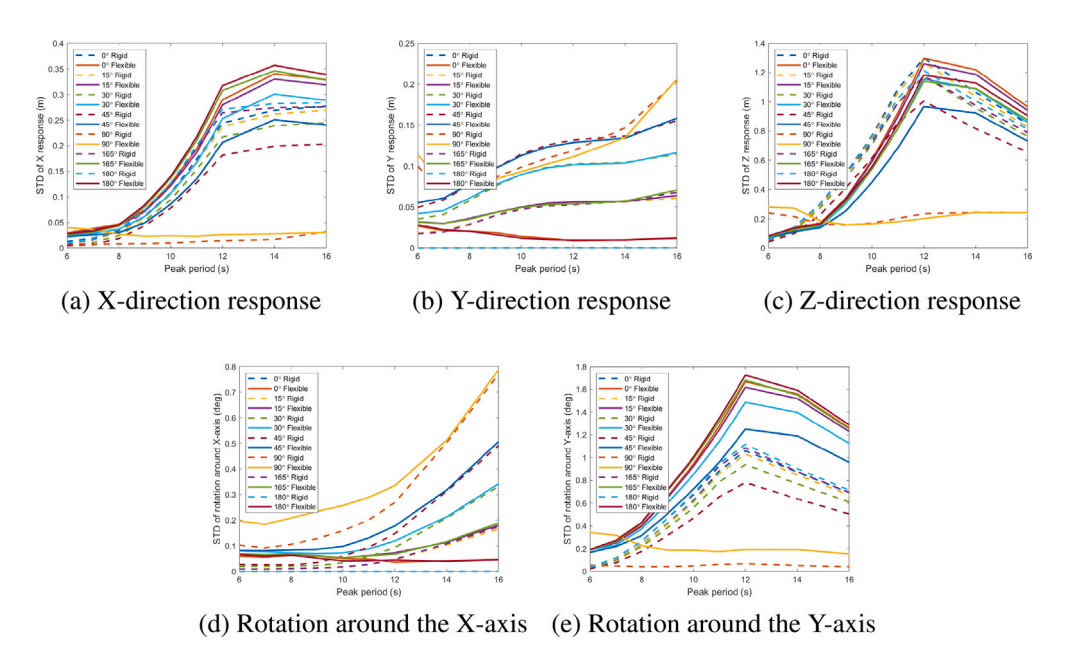


Fig. 22. OWT reference point motions in EC5.

The proposed installation concept is designed to be performed in the following sea condition. Therefore, it is expected that the vessel orientation relative to the spar and the wave directions are selected in a way that this condition is fulfilled. EC5 with varying wave directions and peak periods is defined to investigate wave directions influence. Wave directions other than following or head-sea ( $\beta = 0^{\circ}$  and  $180^{\circ}$  respectively) excite the catamaran vessel's sway, roll, and yaw in addition to surge, heave, and pitch. This results in OWT motions in all 6 DOFs. All the wires used in the current setup coincide at the centroid of the OWT cross-section; therefore, they do not provide stiffness for OWT rotation around Z-axis. Implementing an anti-rotation mechanism inside the collar is expected to eliminate this response in both models. Therefore, the OWT rotation around the Z-axis is eliminated. The results of the OWT reference point are given in Fig. 22.

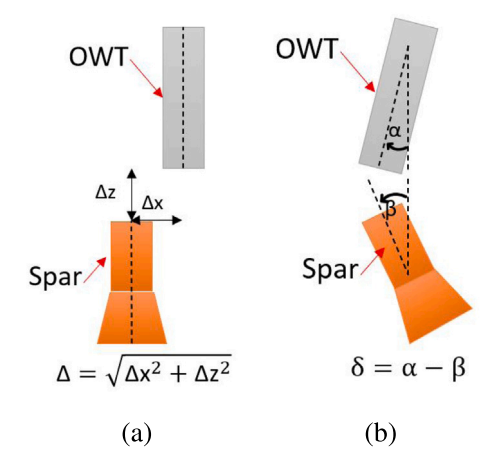


Fig. 23. Relative displacement and alignment definitions in the relative motion between the spar top and OWT bottom: (a) relative displacement definition in 2D, (b) relative alignment definition in 2D.

Analysis shows that having a higher incoming wave angle reduces the transition of the OWT bottom in the X-direction; see Fig. 22(a). This happens as the vessel surge responses become less significant as the wave direction changes 0° to 90°. In addition, the model with flexible crane structures has larger responses than the rigid one.

The OWT bottom transition in Y-direction enlarges as the wave direction changes 0° to 90°; see Fig. 22(b), due to the increase in the vessel sway response. When wave directions are close to the following sea, the model with a flexible crane has a larger response compared to the rigid crane, while this difference reduces as the wave direction gets closer to the beam seas. This happens since the vessel roll motion contribution to the OWT Y-direction transition enlarges by increasing the wave direction.

The OWT Z-direction transition reduces when wave directions vary from  $0^{\circ}$  to  $90^{\circ}$ ; see Fig. 22(c). The pitch response of the catamaran vessel contributes to the OWT Z-direction transition, and when wave directions are getting closer to the beam seas, the catamaran pitch response reduces. The models with rigid cranes have higher Z-direction transitions before the peak at 12 s. After the peak, the model with flexible cranes has larger responses.

The rotation of the OWT bottom around the X-axis enlarges by changing the wave directions from  $0^{\circ}$  to  $90^{\circ}$ , see Fig. 22(d), which is due to the increase in roll motion of the catamaran vessel. The model with flexible cranes has a larger response than the model with rigid cranes. This difference is more significant in lower peak periods and reduces with increasing the peak period.

The rotation of the bottom of OWT around the Y-direction is presented in Fig. 22(e). The responses reduce as the wave direction changes toward beam seas, which is due to the catamaran vessel's pitch motion. The model with flexible cranes has a larger response than the model with rigid cranes. There is a peak at 12 s with the largest difference between the flexible and rigid models, which is in line with the catamaran vessel's pitch natural period.

The OWT bottom responses in the simulations with  $0^{\circ}$  and  $180^{\circ}$  and  $165^{\circ}$  are close to each other. The different shapes of the catamaran's bow and aft introduced minor differences in these two cases. The results are showing that the STD values are higher for transition in the Z-direction and rotation around the X- and Y-directions responses compared to the transition in the X- and Y-directions. Therefore, these OWT responses are expected to have a higher contribution to the relative motion between the OWT and spar.

#### 4.6. Relative motion between the spar top and OWT bottom

The relative motion between the top of the floating spar buoy and the bottom of the hanging OWT is the most significant factor in the mating operation. It is expected that the spar buoy has identical behavior independent of the two models, as there is no mechanical coupling connecting the catamaran vessel to the spar buoy. The relative motion between the two bodies consists of relative displacement and relative alignment. The relative displacement ( $\Delta$ ) is the distance between the spar top and OWT bottom (see Fig. 23(a)), while the relative alignment ( $\delta$ ) is the angle difference between these two (see Fig. 23(b)). An ideal mating operation can be performed by minimizing  $\Delta$  and  $\delta$ .

The time histories of spar top and OWT bottom plane motions, alignment, relative plane motions and relative alignment in EC4 ( $H_s=1$  m and  $T_p=10$  s) with a duration of 100 s are presented in Fig. 24. The inplane motions of the spar top are identical between the rigid and flexible models (see Fig. 24(a)). The governing motion of the spar top is the surge motion, and the heave motion is relatively small. The OWT bottom motions are governed by the Z-direction translation, and the X-direction response is relatively smaller. The pitching of the spar is identical between the two models (see Fig. 24(b)), while the OWT in the flexible model has a higher Y-rotation response compared to the rigid model. From Fig. 24(c), the spread of the horizontal relative displacement for the flexible and rigid cranes is within the range of  $\pm 1$  m. However, the relative vertical displacement has a larger spread for the flexible ( $\pm 1.5$  m) than the rigid crane ( $\pm 1$  m). From Fig. 24(d), the model with flexible cranes presents higher relative alignment compared to the model with rigid cranes.

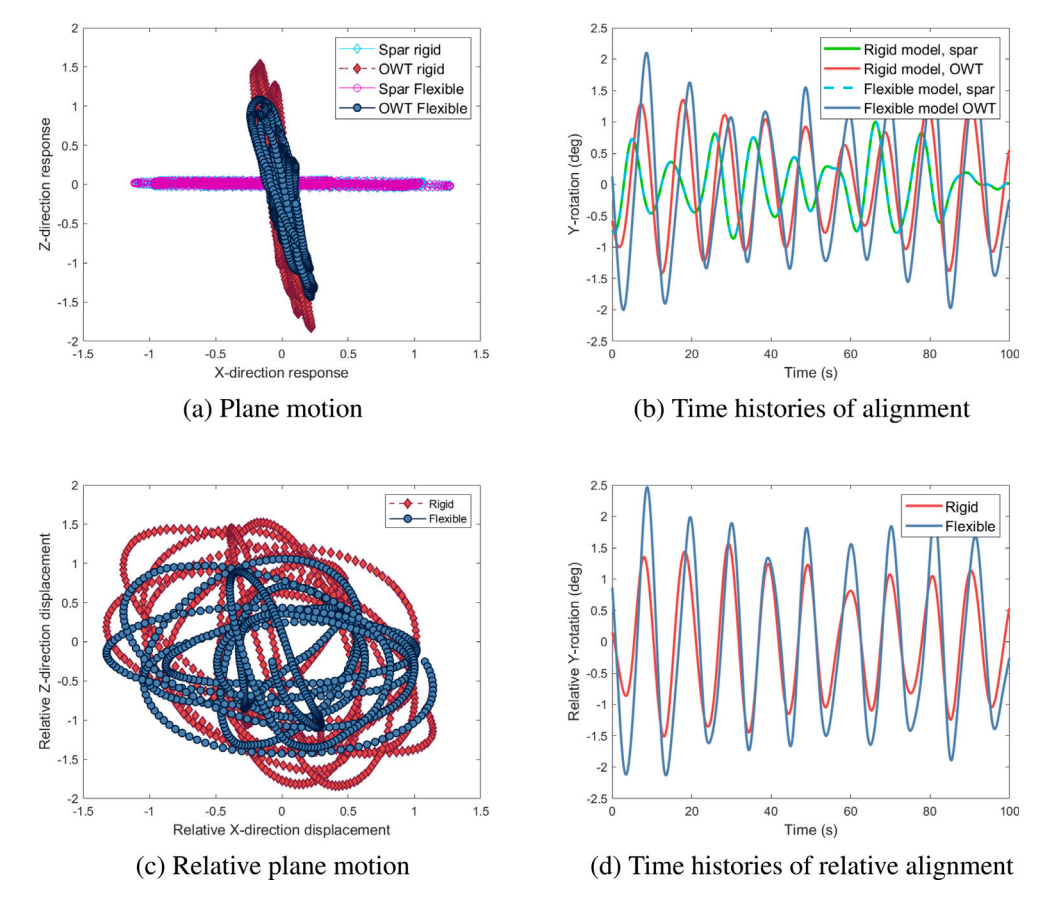


Fig. 24. Time histories of relative plane motions between the spar top and OWT bottom and relative alignment in EC4 ( $H_s = 1$  m and  $T_p = 10$  s).

Since the operation is performed in the following sea condition, the X- and Z-direction transitions and rotation around the Yaxis are the dominant motions contributing to the relative displacement and alignment. The STDs of the relative X- and Z-direction responses, relative displacement and alignment, relative velocity, and relative alignment velocity between the spar top and OWT bottom in EC4 are presented in Fig. 25. The relative displacement (see Fig. 25(c)) is larger for the rigid model for periods less than  $T_n = 12$  s, while the behavior changes after this peak. Relative displacement is driven by both contributions of the X- and Z-direction responses. The relative X-direction response (see Fig. 25(a)) is governed by the surge response of the spar, with a relatively small difference between the rigid and flexible models for  $T_p \le 12$  s. A relatively larger difference is observed for  $T_p > 12$  s with a larger response for the flexible model. The spar buoy surge response has a peak at approximately  $T_p = 14$  s; therefore, enlarged X-direction relative responses are expected within this region for this response. The Z-direction response (see Fig. 25(b)) behaves differently on the two sides of the peak at  $T_p = 12$  s. The model with a rigid crane has a larger Z-direction response for  $T_p < 12$  s, while the model with flexible cranes has a larger response for  $T_p \ge 12$  s. The amplitude of the difference in the Z-direction response is larger than the difference in the X-direction response; therefore, it governs the relative displacement response. The least amount of difference between the flexible and rigid cranes is observed at  $T_p = 12$  and 7 s, which are close to the catamaran heave and pitch natural periods. The flexible cranes have a higher STD for the pitch response in all peak periods (see Fig. 25(d)), and the largest STD difference between the rigid and flexible models is observed for this motion. The catamaran vessel has a natural pitch period of approximately 12 s; therefore, it is expected to see the peak of the relative alignment at this frequency.

Two measures can be taken to reduce the relative motion between the spar and the OWT.

- 1. Implementing control systems on the winches allows the reduction of the lifted preassembly motion and, as a result, reduces the relative motion, for example, by actively controlling the lifting and stabilizing wire lengths [33,48].
- 2. Another measure is by utilizing a mechanical coupling between the installation vessel and the floating substructure. For example, implementing fender and winch couplings between the installation vessel and floating substructures reduces the relative motion [49]".

The relative velocities between the spar top and the OWT bottom are demonstrated in Figs. 25(e) and 25(f) in EC4. Connection device design is dependent on these results, as the impact forces govern the design of the current bolted connections. However, the OWT industry can benefit from more innovative connection solutions. Up to  $T_p = 8$  s, models with flexible and rigid cranes exhibit

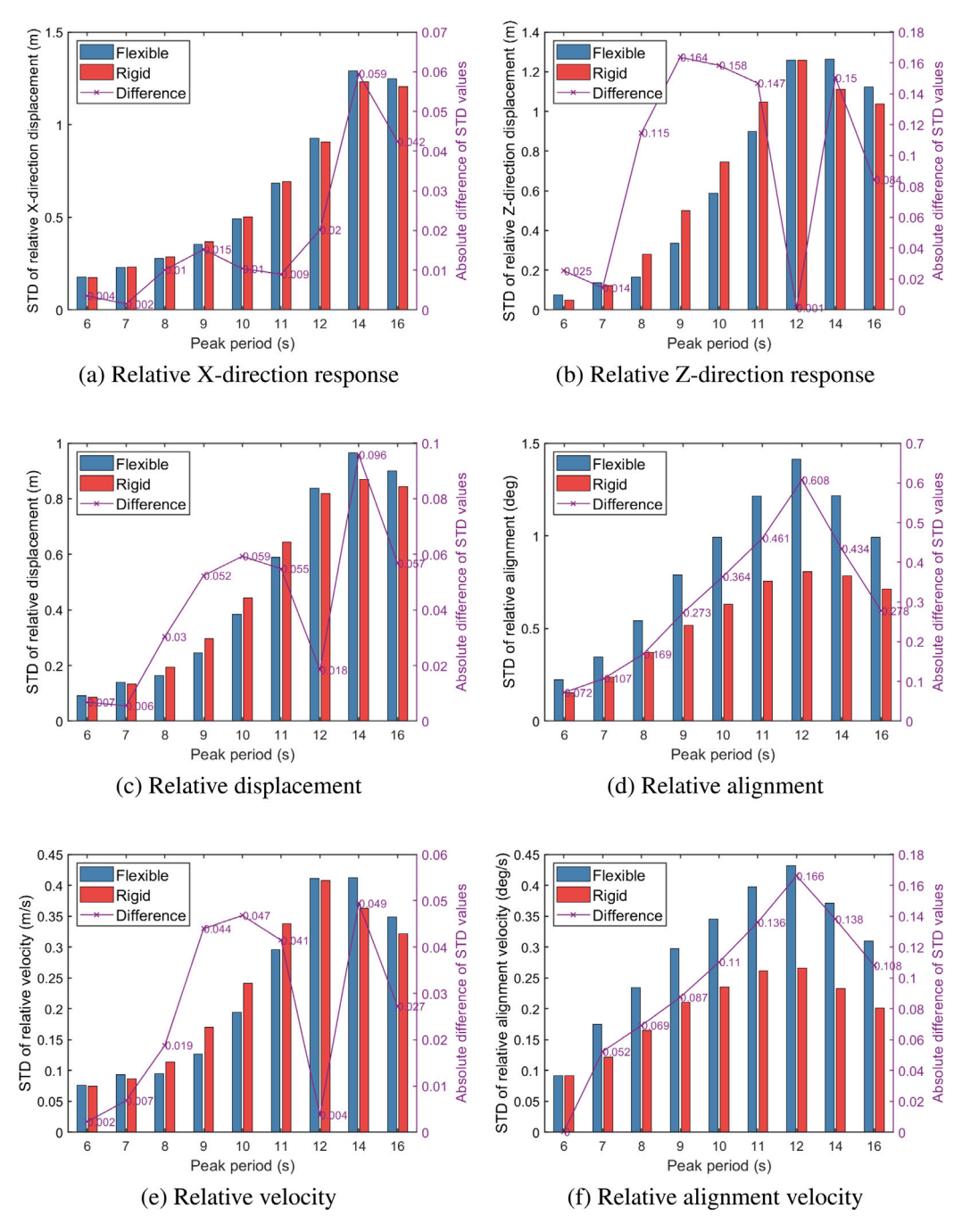


Fig. 25. Relative displacement and alignment between the spar top and OWT bottom in EC4.

similar behavior in relative velocity. In higher periods up to  $T_p = 12$  s, the model with rigid cranes has a higher velocity, and the behavior changes after this peak. The alignment velocity has a peak at  $T_p = 12$  s (catamaran's pitch natural period), and the model with the flexible cranes has a higher response in all period ranges.

The power spectrum for the relative motions and alignment between the OWT and spar top in EC4,  $H_s = 1$  m and  $T_p = 10$  s, is presented in Fig. 26. Both models have similar behavior with a slightly larger response for the rigid model for the relative X-direction. Two peaks are observed at approximately 10 s and 12 s, which are governed by the wave period and the catamaran pitch natural period. The Z-direction for the rigid model has a larger response as the power curves contain more energy; however, for the flexible model, the peak is shifted toward higher periods. Therefore, pitch coupling has a larger influence on this model. The

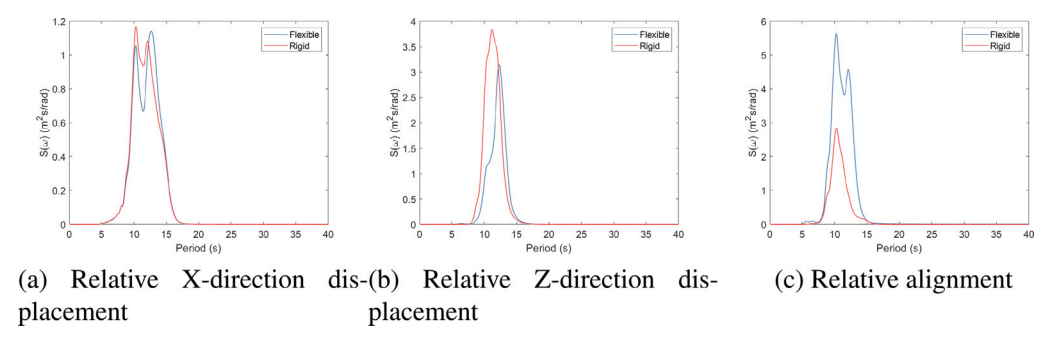


Fig. 26. Relative motion spectra between the spar top and OWT bottom in EC4,  $H_x = 1$  m,  $T_p = 10$  s.

relative alignment between the bodies is governed by the wave period and the catamaran pitch natural period at 12 s, with a larger response for the flexible model.

#### 5. Conclusion and future work

#### 5.1. Conclusions

Offshore wind turbine installation operations are complicated from both technical and commercial points of view. Often, the OWT industry introduces strict guidelines for mating operations with low margins on the relative motion between an OWT and a floating substructure (spar buoy). Most of the research assumes the crane structure to be a rigid body, and the effect of the crane flexibility is rarely discussed in the literature. This paper fills this gap by evaluating the effect of crane structure stiffness on mating operations. The proposed low-height lifting mechanism by SFI-MOVE consists of cranes, wires, winches, and controllers that allow the installation operation to be performed from the bottom rather than conventional top lifting. In this article, simplifications are performed to develop a deeper understanding of the underlying system dynamics. In this simplification procedure, the initial 3D frame crane structures are replaced with equivalent beams, controllers are deactivated, and the height of crane structures is increased to eliminate the inverted pendulum behavior. Numerical models are developed to simulate the operations. The study compares the responses from two different models of the crane structure, one where the crane is a rigid part of the catamaran installation vessel and one where the flexibility of the crane is included by using finite beam elements to represent the crane structure. Comparison work under different wave conditions is performed between the rigid and flexible multibody dynamics. It is concluded that:

- Crane structure flexibility affects the vessel-crane-OWT coupled dynamics. This coupling changes the catamaran RAO, shifts the natural periods and enlarges the response amplitudes.
- The catamaran vessel response, crane structure displacements, wire tensions, and OWT bottom motions have a linear relationship with the wave amplitudes. Differences were observed in these responses between the two flexible and rigid models, and the differences increased at higher wave amplitudes. The X-direction response of the OWT bottom is an exception, as the two models behave similar to each other at higher excitation levels.
- · Introducing the crane structural flexibility modifies the responses compared to the rigid crane:
  - Cranes top X- and Z-direction responses depends on the wave frequency. The rigid crane model does not provide any response for the Y-direction response.
  - Lifting wire tensions have the same mean in both models (equivalent to the OWT weight), while the flexible model has
    a higher STD. The mean of stabilizing wire tensions is frequency dependent, while the flexible model has higher STDs.
     For surge wires the rigid model has a higher mean tension than the flexible model, while the flexible model has a higher
    STD.
  - Flexible cranes have larger OWT bottom responses for transition in the X-direction and rotation around the *Y*-axis. The Z-direction response is dependent on the excitation frequency.
- The longitudinal relative displacement between the OWT bottom and spar top is governed by the surge motion of the spar. The vertical relative displacement between the OWT bottom and spar top is governed by the catamaran heave and pitch responses.
- Relative displacement and alignment and their corresponding velocities have peaks at the catamarans and spars natural periods
  for both rigid and flexible models. The smallest differences in relative displacements and velocities are evaluated between the
  two rigid and flexible models at the catamaran heave and natural periods.
- Relative alignment between the OWT and spar has the most significant difference between the flexible and rigid models. Furthermore, the catamaran installation vessel pitch motion governed the response pattern.
- As natural periods of the catamaran vessel, lifting assembly can occur within the frequency range of the wave spectrum.
   Therefore, it is recommended to perform the OWT installation simulation considering the crane structure flexibility, as it provides a more realistic analysis.

#### 5.2. Recommendations for future work

In the present research, the effect of structural flexibility is estimated for the installation of OWT units using a low-height lifting mechanism. Controllers are deactivated to develop a deeper understanding of the dominant dynamic behaviors in the system. The height of the lifting cranes is increased to stabilize the dynamics and eliminate the inverse pendulum behavior of the OWT. Controllers can be implemented in future research, and interactions between controllers can be investigated.

Regular and irregular waves are forced to the system as environmental forces, while generalized feasibility studies can be performed by exerting currents and winds in addition to ocean waves. Only first-order wave effects are considered in this research, while wave drift forces might have a severe effect on the spar and catamaran; therefore, this topic should be addressed as a follow-up to the current work.

The proposed system consists of multiple components, and one recommendation is to model such an operation with a modular approach. The functional mockup interface [50] standard can be utilized for modularized modeling with possibilities for cosimulation and model exchange. Another advantage of this approach could be the future development of every component, such as advanced controllers and DP systems.

Mating OWTs is a sea-estate-sensitive operation, and today's industry suffers from a lack of innovative connection devices. Therefore, the relative velocities between the bodies are estimated in the current research in addition to the relative motions. These results can be used to overcome the challenges by estimating impact forces and designing possible quick connection devices.

#### **Declaration of competing interest**

The authors declare that they have no known competing financial interests or personal relationships that could have appeared to influence the work reported in this paper.

#### Data availability

Data will be made available on request.

#### Acknowledgments

This work was supported by the Research Council of Norway (RCN) through the Centre for Research-based Innovation on Marine Operations (SFI MOVE, RCN-project 237929).

# References

- [1] Ritchie H, Roser M. Energy. Our World in Data 2020. https://ourworldindata.org/energy.
- [2] Commission E. A clean planet for all a European strategic long-term vision for a prosperous, modern, competitive and climate neutral economy. 2018.
- [3] GWEC. Global wind report 2021. 2021.
- [4] Manwell JF. Wind energy explained: theory, design and application. 2009.
- [5] Geng Z, Xie Y, Zhuang L, Burla M, Hoekman M, Roeloffzen CGH, et al. Photonic integrated circuit implementation of a sub-GHz-selectivity frequency comb filter for optical clock multiplication. Opt Express 2017;25(22):27635–45. http://dx.doi.org/10.1364/OE.25.027635, URL https://opg.optica.org/oe/abstract.cfm?URI=oe-25-22-27635.
- [6] Stewart G, Muskulus M. A review and comparison of floating offshore wind turbine model experiments. Energy Procedia 2016;94:227–31. http://dx.doi.org/10.1016/j.egypro.2016.09.228, 13th Deep Sea Offshore Wind R&D Conference, EERA DeepWind'2016. URL https://www.sciencedirect.com/science/article/pii/S1876610216309146.
- [7] Europe W. Offshore wind in europe, key trends and statistics 2020. 2021.
- [8] Ren Z, Jiang Z, Gao Z, Skjetne R. Active tugger line force control for single blade installation. Wind Energy (Chichester, England) 2018;21(12):1344-58.
- [9] Zhao Y, Cheng Z, Gao Z, Sandvik PC, Moan T. Numerical study on the feasibility of offshore single blade installation by floating crane vessels. Mar Struct 2019;64:442–62. http://dx.doi.org/10.1016/j.marstruc.2018.12.001, URL https://www.sciencedirect.com/science/article/pii/S0951833918302272.
- [10] Zhao Y, Cheng Z, Sandvik PC, Gao Z, Moan T, Van Buren E. Numerical modeling and analysis of the dynamic motion response of an offshore wind turbine blade during installation by a jack-up crane vessel. Ocean Eng 2018;165:353–64.
- [11] Ren Z, Jiang Z, Skjetne R, Gao Z. Development and application of a simulator for offshore wind turbine blades installation. Ocean Eng 2018;166:380–95. http://dx.doi.org/10.1016/j.oceaneng.2018.05.011, URL https://www.sciencedirect.com/science/article/pii/S0029801818307224.
- [12] Ren Z, Han X, Yu X, Skjetne R, Leira BJ, Sævik S, et al. Data-driven simultaneous identification of the 6DOF dynamic model and wave load for a ship in waves. Mech Syst Signal Process 2023;184:109422. http://dx.doi.org/10.1016/j.ymssp.2022.109422, URL https://www.sciencedirect.com/science/article/pii/S0888327022005441
- [13] Verma AS, Jiang Z, Vedvik NP, Gao Z, Ren Z. Impact assessment of a wind turbine blade root during an offshore mating process. Eng Struct 2019;180:205–22. http://dx.doi.org/10.1016/j.engstruct.2018.11.012, URL https://www.sciencedirect.com/science/article/pii/S0141029618315657.
- [14] Verma AS, Jiang Z, Gao Z, Vedvik NP. Effects of a passive tuned mass damper on blade root impacts during the offshore mating process. Mar Struct 2020;72:102778. http://dx.doi.org/10.1016/j.marstruc.2020.102778, URL https://www.sciencedirect.com/science/article/pii/S0951833920300721.
- [15] Jiang Z, Li L, Gao Z, Halse KH, Sandvik PC. Dynamic response analysis of a catamaran installation vessel during the positioning of a wind turbine assembly onto a spar foundation. Mar Struct 2018;61:1–24. http://dx.doi.org/10.1016/j.marstruc.2018.04.010, URL https://www.sciencedirect.com/science/article/pii/S0951833917303374.
- [16] Ulstein. Windlifter. 2021, URL https://ulstein.com/equipment/ulstein-windlifter.
- [17] Jiang Z, Yttervik R, Gao Z, Sandvik PC. Design, modelling, and analysis of a large floating dock for spar floating wind turbine installation. Mar Struct 2020;72:102781. http://dx.doi.org/10.1016/j.marstruc.2020.102781, URL https://www.sciencedirect.com/science/article/pii/S0951833920300757.
- [18] Cha J-H, Roh M-I, Lee K-Y. Dynamic response simulation of a heavy cargo suspended by a floating crane based on multibody system dynamics. Ocean Eng 2010;37(14):1273–91.

[19] Cheng X, Li G, Skulstad R, Major P, Chen S, Hildre HP, et al. Data-driven uncertainty and sensitivity analysis for ship motion modeling in offshore operations. Ocean Eng 2019:179:261-72.

- [20] Lee H-W, Roh M-I, Ham S-H, Ku N-K. Coupled analysis method of a mooring system and a floating crane based on flexible multibody dynamics considering contact with the seabed. Ocean Eng 2018;163:555–69. http://dx.doi.org/10.1016/j.oceaneng.2018.06.025, URL https://www.sciencedirect.com/science/article/pii/S0029801818310497.
- [21] Yang C, Du J, Cheng Z, Wu Y, Li C. Flexibility investigation of a marine riser system based on an accurate and efficient modelling and flexible multibody dynamics. Ocean Eng 2020;207:107407. http://dx.doi.org/10.1016/j.oceaneng.2020.107407, URL https://www.sciencedirect.com/science/article/pii/S0029801820304352.
- [22] Guo Y-T, Nie X, Fan J-S, Tao M-X. Shear resistance of steel-concrete-steel deep beams with bidirectional webs. Steel Compos Struct 2022;42(3):299–313. http://dx.doi.org/10.12989/scs.2022.42.3.299.
- [23] Guo Y-T, Nie X, Tao M-X, Ding R, Tang L, Fan J-S. Selected series method on buckling design of stiffened steel-concrete composite plates. J Construct Steel Res 2019;161:296–308. http://dx.doi.org/10.1016/j.jcsr.2019.07.014.
- [24] Xie C, Zhou L, Ding S, Liu R, Zheng S. Experimental and numerical investigation on self-propulsion performance of polar merchant ship in brash ice channel. Ocean Eng 2023;269:113424. http://dx.doi.org/10.1016/j.oceaneng.2022.113424, URL https://www.sciencedirect.com/science/article/pii/S002980182202707X
- [25] Park K-P, Cha J-H, Lee K-Y. Dynamic factor analysis considering elastic boom effects in heavy lifting operations. Ocean Eng 2011;38(10):1100-13.
- [26] Wang L, Kolios A, Cui L, Sheng Q. Flexible multibody dynamics modelling of point-absorber wave energy converters. Renew Energy 2018;127:790–801. http://dx.doi.org/10.1016/j.renene.2018.05.029, URL https://www.sciencedirect.com/science/article/pii/S0960148118305500.
- [27] Helsen J, Marrant B, Vanhollebeke F, Coninck FD, Berckmans D, Vandepitte D, et al. Assessment of excitation mechanisms and structural flexibility influence in excitation propagation in multi-megawatt wind turbine gearboxes: Experiments and flexible multibody model optimization. Mech Syst Signal Process 2013;40(1):114–35. http://dx.doi.org/10.1016/j.ymssp.2012.12.001, URL https://www.sciencedirect.com/science/article/pii/S0888327012004700.
- [28] Nada AA, Al-Shahrani AS. Shape optimization of low speed wind turbine blades using flexible multibody approach. Energy Procedia 2017;134:577–87. http://dx.doi.org/10.1016/j.egypro.2017.09.567, sustainability in Energy and Buildings 2017: Proceedings of the Ninth KES International Conference, Chania, Greece, 5–7 July 2017. URL https://www.sciencedirect.com/science/article/pii/S187661021734701X.
- [29] Al-Solihat MK, Nahon M. Flexible multibody dynamic modeling of a floating wind turbine. Int J Mech Sci 2018;142–143:518–29. http://dx.doi.org/10. 1016/j.ijmecsci.2018.05.018, URL https://www.sciencedirect.com/science/article/pii/S0020740317305015.
- [30] NTNU. Marine operations move. 2022, URL https://www.ntnu.edu/move.
- [31] Zhang L, Shi W, Zeng Y, Michailides C, Zheng S, Li Y. Experimental investigation on the hydrodynamic effects of heave plates used in floating offshore wind turbines. Ocean Eng 2023;267:113103. http://dx.doi.org/10.1016/j.oceaneng.2022.113103, URL https://www.sciencedirect.com/science/article/pii/S0029801822023861.
- [32] Vagnes D, Monteiro TG, Halse KH, Hildre HP. Low-height lifting system for offshore wind turbine installation: modelling and hydrodynamic response analysis using the commercial simulation tool sima. In: OMAE2020, editor. Proceedings of the ASME 39th international conference on ocean, offshore and arctic engineering. Fort Lauderdale, FL,USA: ASME; 2020, an optional note.
- [33] Ren Z, Verma AS, Ataei B, Halse KH, Hildre HP. Model-free anti-swing control of complex-shaped payload with offshore floating cranes and a large number of lift wires. Ocean Eng 2021;228:108868. http://dx.doi.org/10.1016/j.oceaneng.2021.108868, URL https://www.sciencedirect.com/science/article/pii/ S0029801821003036
- [34] Xu J, Ataei B, Halse KH, Hildre HP, Mikalsen ET. Virtual prototyping of a low-height lifting system for offshore wind turbine installation. In: OMAE2020, editor. Proceedings of the ASME 39th international conference on ocean, offshore and arctic engineering. Fort Lauderdale, FL,USA: ASME; 2020, an optional
- [35] Sintef. Sima. 2020, URL https://www.sintef.no/en/software/sima/.
- [36] SAIPEM, HYWIND, 2022, URL https://www.saipem.com/en/projects/hywind.
- [37] DNV. Recommended practice DNV-RP-h103, modelling and analysis of marine operations. 2011.
- [38] Equinor. The future of offshore wind is afloat. 2021, URL https://www.equinor.com/en/what-we-do/floating-wind.html.
- [39] Jiang Z. Installation of offshore wind turbines: A technical review. Renew Sustain Energy Rev 2021;139:110576. http://dx.doi.org/10.1016/j.rser.2020. 110576, URL https://www.sciencedirect.com/science/article/pii/S1364032120308601.
- [40] Faltinsen OM. Sea loads on ships and offshore structures. 1990.
- [41] Equinor. Hywind Scotland. 2017, URL https://www.equinor.com/en/what-we-do/floating-wind/hywind-scotland.html.
- [42] Liu T, Halse KH, Leira BJ, Jiang Z. Comparative study of the mating process for a spar-type floating wind turbine using two alternative installation vessels. Appl Ocean Res 2023;132:103452. http://dx.doi.org/10.1016/j.apor.2022.103452, URL https://www.sciencedirect.com/science/article/pii/S0141118722003819.
- [43] Hong S, Zhang H, Nord TS, Halse KH. Effect of fender system on the dynamic response of onsite installation of floating offshore wind turbines. Ocean Eng 2022;259:111830. http://dx.doi.org/10.1016/j.oceaneng.2022.111830, URL https://www.sciencedirect.com/science/article/pii/S0029801822011738.
- [44] Bak C, Zahle F, Bitsche R, Kim T, Yde A, Henriksen LC, et al. Description of the DTU 10 MW reference wind turbine. 2013.
- [45] Ocean S. SIMO 4.20.2 theory manual. 2021.
- [46] Ocean S. RIFLEX 4.20.2 theory manual. 2021
- [47] DNV. Recommended practice DNV-RP-c205, environmental conditions and environmental loads. 2010.
- [48] Ren Z, Zhen X, Jiang Z, Gao Z, Li Y, Shi W. Underactuated control and analysis of single blade installation using a jackup installation vessel and active tugger line force control. Mar Struct 2023;88:103338. http://dx.doi.org/10.1016/j.marstruc.2022.103338.
- [49] Liu T, Halse KH, Leira BJ, Jiang Z, Chai W, Brathaug H-P, et al. Dynamic response of a SWATH vessel for installing pre-assembled floating wind turbines. Mar Struct 2023;88:103341. http://dx.doi.org/10.1016/j.marstruc.2022.103341, URL https://www.sciencedirect.com/science/article/pii/S0951833922001770.
- [50] FMI. Functional mock-up interface. 2021, URL https://fmi-standard.org/.